

Many-particle hydrodynamic interactions in parallel-wall geometry: Cartesian-representation method

S. Bhattacharya, J. Blawdziewicz, and E. Wajnryb¹

*Department of Mechanical Engineering, Yale University, New Haven, CT
06520-8286, USA*

Abstract

This paper describes the results of our theoretical and numerical studies of hydrodynamic interactions in a suspension of spherical particles confined between two parallel planar walls, under creeping-flow conditions. We propose a novel algorithm for accurate evaluation of the many-particle friction matrix in this system—no such algorithm has been available so far.

Our approach involves expanding the fluid velocity field into spherical and Cartesian fundamental sets of Stokes flows. The interaction of the fluid with the particles is described using the spherical basis fields; the flow scattered with the walls is expressed in terms of the Cartesian fundamental solutions. At the core of our method are transformation relations between the spherical and Cartesian basis sets. These transformations allow us to describe the flow field in a system that involves both the walls and particles.

We used our accurate numerical results to test the single-wall superposition approximation for the hydrodynamic friction matrix. The approximation yields fair results for quantities dominated by single particle contributions, but it fails to describe collective phenomena, such as a large transverse resistance coefficient for linear arrays of spheres.

1 Introduction

Equilibrium and nonequilibrium behavior of colloidal suspensions in confined geometries has recently been extensively discussed. Examples of recent papers include experimental studies of particle deposition on chemically patterned

¹ On leave from IPPT Warsaw, Poland

planar walls [1], investigations of collective dynamics in quasi-bidimensional suspensions in slit pores [2, 3, 4], and observations of drainage behavior of particle-stabilized thin liquid films [5]. The research has been stimulated, in part, by emerging applications—such as microfluidic devices and production of photonic materials by self-assembly of colloidal crystals [6, 7]. The investigations have also been considerably influenced by development of new experimental techniques, including the evanescent-wave microscopy [8, 9], computerized video microscopy [10, 11, 4, 12], and optical tweezers [13].

While the equilibrium structure of confined colloidal suspensions is fully determined by the particle–wall and interparticle interaction potentials, the dynamics is also significantly affected by the many-body hydrodynamic forces. The effect of the hydrodynamic interactions on particle motion can be expressed in terms of the N -particle friction and mobility matrices [14], which depend on the particle positions and the wall geometry.

For spherical particles in an unbounded space, efficient algorithms for evaluation of the friction and mobility matrices have been developed [15, 16, 17, 18, 19]. The algorithms combine multipolar expansion methods with the lubrication approximation for particles in close proximity [15]. This approach has recently been generalized by Cichocki et al. [20, 21] to systems of particles bounded by a single planar wall; the particle–wall hydrodynamic interactions were included using the image representation of the flow reflected from the wall [20].

Much less progress has been made for suspensions confined between two planar walls (e.g, in a slit pore, or between two glass plates). For a single particle, several *ad hoc* approximations for the mobility matrix have been proposed [22, 23], and numerical results obtained by boundary-integral methods are available [24, 25, 26]. Recently, we have developed an exact image representation of the flow between two walls [27], which allows accurate evaluation of the single-particle friction matrix by a multipolar expansion technique. However, none of the above methods has been generalized to multiparticle systems, due to a large numerical cost of boundary-integral calculations or the slow convergence of the image solutions.

Two extensions of the free-space Stokesian-dynamics algorithm [15] to wall bounded systems have been proposed by Brady and his collaborators [28, 29, 30]. In the first approach the walls are discretized [28], and in the second they are modeled as static, closely packed arrays of spheres [29, 30]. The first method has not been further explored. The results obtained using the second method are only qualitative, because the walls are porous and rough.

To overcome the above-mentioned problems, we adopt here an alternative ap-

proach, based on Fourier analysis of the flow field reflected from the walls.² According to our method, the flow field in the system is expanded using two basis sets of solutions of Stokes equations—the spherical and the Cartesian basis. The spherical basis is used for a description of the flow field scattered from the particles, and the Cartesian basis is appropriate for the wall geometry. The key result of our study is a set of transformation formulas for conversion between the spherical and Cartesian representations. The transformation formulas allow to evaluate the spherical matrix elements of the Green function for Stokes flow in the presence of the walls in terms of simple two-dimensional Fourier integrals.

The results of our theoretical analysis have been implemented in a numerical procedure for evaluating multi-particle hydrodynamic interactions in a suspension of spheres confined between two planar walls. The procedure combines the expansions of the flow field into the spherical and Cartesian basis fields with the two-particle superposition approximation for the friction matrix, in order to include slowly convergent lubrication corrections. Since the force multipoles induced on particle surfaces are included to arbitrary order, highly accurate results are obtained.

Examples of numerical results for two-particle and many-particle systems are provided. In particular, our results illustrate the role of the far-field flow produced in the space between the walls by the moving particles. We show that the single-wall superposition approximation does not correctly describe the far-field flow, and thus it fails to capture some important collective phenomena such as the increased hydrodynamic resistance due to the backflow produced by the moving particles.

This paper is organized as follows. In Section 2 we summarize the induced-force formulation of the Stokes-flow equations for a multiparticle system in the wall presence. In Section 3 the induced-force equations are transformed into an infinite array of algebraic equations for the induced-force multipoles, using a multipolar expansion of Stokes flow.

Our main theoretical results are presented in Sections 4–7. In Section 4 the Cartesian basis sets of Stokes flows are defined, and the transformation formulas for conversion between the Cartesian and the spherical multipolar bases sets are derived. The displacement and conversion formulas are then used to obtain two-dimensional Fourier representations of the matrix elements of Green operator for infinite space (Section 5), halfspace bounded by a single wall (Section 6), and a region bounded by two parallel planar walls (Section 7).

² Recently, investigations along similar lines have also been reported by Jones [31, 32].

A numerical algorithm for computation of hydrodynamic interactions in a suspension of spheres confined in a region bounded by two parallel walls is described in Section 8. Numerical examples of the friction matrix, evaluated using this algorithm, are given in Section 9. Directions for further development of our method are indicated in the concluding Section 10. Some technical details are presented in Appendices A–D.

2 Induced-force formulation

We consider a suspension of N spherical particles of radius a moving in an incompressible Newtonian fluid of viscosity η . The suspension is bounded by a single planar wall or two parallel planar walls. The creeping-flow conditions are assumed; therefore, the fluid flow in the system depends only on the instantaneous particle configuration and velocities. The configuration is described by the positions $(\mathbf{R}_1, \dots, \mathbf{R}_N)$ of particle centers. The translational and rotational velocities of the particles are \mathbf{U}_i and $\mathbf{\Omega}_i$, where $i = 1, \dots, N$.

The effect of the suspended particles on the surrounding fluid can be described in terms of the induced force distributions on the particle surfaces

$$\mathbf{F}_i(\mathbf{r}) = a^{-2} \delta(r_i - a) \mathbf{f}_i(\mathbf{r}), \quad (1)$$

where

$$\mathbf{r}_i = \mathbf{r} - \mathbf{R}_i \quad (2)$$

and $r_i = |\mathbf{r}_i|$. By definition of the induced force, the flow field

$$\mathbf{v}(\mathbf{r}) = \mathbf{v}^{\text{ext}} + \sum_{i=1}^N \int \mathbf{T}(\mathbf{r}, \mathbf{r}') \cdot \mathbf{F}_i(\mathbf{r}') d\mathbf{r}' \quad (3)$$

is identical to the velocity field in the presence of the particles [33, 34, 35]. In the above equation, \mathbf{v}^{ext} denotes the imposed flow, and the integral term describes the flow generated by the induced forces. Here

$$\mathbf{T}(\mathbf{r}, \mathbf{r}') = \mathbf{T}_0(\mathbf{r} - \mathbf{r}') + \mathbf{T}'(\mathbf{r}, \mathbf{r}') \quad (4)$$

is the Green function for the Stokes flow in the presence of the boundaries,

$$\mathbf{T}_0(\mathbf{r}) = \frac{1}{8\pi\eta r} (\hat{\mathbf{I}} + \hat{\mathbf{r}}\hat{\mathbf{r}}) \quad (5)$$

denotes the Oseen tensor (where $\hat{\mathbf{I}}$ is the identity tensor, and $\hat{\mathbf{r}} = \mathbf{r}/r$), and $\mathbf{T}'(\mathbf{r}, \mathbf{r}')$ describes the flow reflected from the walls.

The induced force distribution \mathbf{F}_i on the surface of particle i and the flow \mathbf{v}_i^{in} incident to this particle are linearly related. The relation can be expressed in

the form

$$\mathbf{F}_i = -\mathbf{Z}_i(\mathbf{v}_i^{\text{in}} - \mathbf{v}_i^{\text{rb}}), \quad (6)$$

where

$$\mathbf{v}_i^{\text{rb}}(\mathbf{r}) = \mathbf{U}_i + \boldsymbol{\Omega}_i \times \mathbf{r}_i \quad (7)$$

denotes the rigid-body velocity field corresponding to the particle motion, and

$$\bar{\mathbf{v}}_i^{\text{in}} = \mathbf{v}_i^{\text{in}} - \mathbf{v}_i^{\text{rb}} \quad (8)$$

is the incident flow in the reference frame moving with the particle. The Stokes flow field (8) is fully determined by its boundary value on the particle surface S_i and the condition that $\bar{\mathbf{v}}_i^{\text{in}}$ is nonsingular in the region occupied by the particle. Thus, (6) can be interpreted as a linear functional relation between the vector fields (1) and (8) specified on the surface S_i . Since a nonzero flow (8) always produces a nonzero force distribution \mathbf{F}_i , relation (6) can be inverted

$$\mathbf{v}_i^{\text{in}} - \mathbf{v}_i^{\text{rb}} = -[\mathbf{Z}_i^{-1}\mathbf{F}_i](\mathbf{r}), \quad \mathbf{r} \in S_i. \quad (9)$$

For specific particle models, explicit expressions for the operator \mathbf{Z}_i are obtained by solving Stokes equations for an isolated particle subject to an external flow in an unbounded fluid [36, 37, 38].

The flow \mathbf{v}_i^{in} incident to a particle i in a multiparticle system is defined by the equation

$$\mathbf{v}(\mathbf{r}) = \mathbf{v}_i^{\text{in}}(\mathbf{r}) + \mathbf{v}_i^{\text{out}}(\mathbf{r}), \quad (10)$$

where $\mathbf{v}(\mathbf{r})$ is the total flow (3), and

$$\mathbf{v}_i^{\text{out}}(\mathbf{r}) = \int \mathbf{T}_0(\mathbf{r} - \mathbf{r}') \cdot \mathbf{F}_i(\mathbf{r}') d\mathbf{r}' \quad (11)$$

represents the flow scattered by the considered particle. By collecting relations (9)–(11) we obtain the expression

$$\mathbf{v}(\mathbf{r}) = \mathbf{v}_i^{\text{rb}}(\mathbf{r}) - [\mathbf{Z}_i^{-1}\mathbf{F}_i](\mathbf{r}) + \int \mathbf{T}_0(\mathbf{r} - \mathbf{r}') \cdot \mathbf{F}_i(\mathbf{r}') d\mathbf{r}', \quad \mathbf{r} \in S_i, \quad (12)$$

for the flow at the surface S_i of the particle i . For rigid spheres, the velocity field $\mathbf{v}(\mathbf{r})$ in equation (12) satisfies the no-slip boundary condition

$$\mathbf{v}(\mathbf{r}) = \mathbf{v}_i^{\text{rb}}(\mathbf{r}), \quad \mathbf{r} \in S_i. \quad (13)$$

Accordingly, we have the identity [21]

$$[\mathbf{Z}_i^{-1}\mathbf{F}_i](\mathbf{r}) = \int \mathbf{T}_0(\mathbf{r} - \mathbf{r}') \cdot \mathbf{F}_i(\mathbf{r}') d\mathbf{r}', \quad \mathbf{r} \in S_i \quad (14)$$

for such particles.

By combining expressions (3) and (12), we get the boundary-integral equation for the induced force densities \mathbf{F}_i ,

$$[\mathbf{Z}_i^{-1}\mathbf{F}_i](\mathbf{r}) + \sum_{j=1}^N \int [(1 - \delta_{ij})\mathbf{T}_0(\mathbf{r} - \mathbf{r}') + \mathbf{T}'(\mathbf{r}, \mathbf{r}')] \cdot \mathbf{F}_j(\mathbf{r}') d\mathbf{r}' = \mathbf{v}_i^{\text{rb}}(\mathbf{r}) - \mathbf{v}^{\text{ext}}(\mathbf{r}),$$

$$\mathbf{r} \in S_i. \quad (15)$$

In the following sections, equation (15) is transformed into an infinite set of algebraic equations for the multipole moments of the induced force, with coefficients expressed in terms of two-dimensional Fourier integrals.

3 Matrix representation

3.1 Spherical basis

The matrix representation of equation (15) is obtained by expanding fluid velocity fields into sets of fundamental solutions of Stokes equations in spherical coordinates, and expressing the induced-force distributions in terms of the corresponding force multipoles. In our analysis we employ sets of basis fields that are closely related to the sets introduced by Cichocki et al. [37]; we use, however, a different normalization to emphasize important symmetries of the problem.

The singular and nonsingular basis sets of solutions of Stokes equations $\mathbf{v}_{lm\sigma}^{-}(\mathbf{r})$ and $\mathbf{v}_{lm\sigma}^{+}(\mathbf{r})$ (where $l = 1, 2, \dots$; $m = -l, \dots, l$; and $\sigma = 0, 1, 2$) are defined by the following conditions: (i) the basis velocity fields are homogeneous functions of the radial variable r ,

$$\mathbf{v}_{lm\sigma}^{-}(\mathbf{r}) = \mathbf{V}_{lm\sigma}^{-}(\theta, \phi)r^{-(l+\sigma)}, \quad (16)$$

$$\mathbf{v}_{lm\sigma}^{+}(\mathbf{r}) = \mathbf{V}_{lm\sigma}^{+}(\theta, \phi)r^{l+\sigma-1}, \quad (17)$$

where (r, θ, ϕ) represent the vector \mathbf{r} in spherical coordinates; (ii) the coefficients $\mathbf{V}_{lm\sigma}^{-}(\theta, \phi)$ and $\mathbf{V}_{lm\sigma}^{+}(\theta, \phi)$ are combinations of vector spherical harmonics with angular order l and azimuthal order m ; and (iii) the basis velocity fields $\mathbf{v}_{lm\sigma}^{\pm}(\mathbf{r})$ satisfy the following hierarchies of curl relations

$$\mathbf{v}_{lm1}^{-} = -i\nabla \times \mathbf{v}_{lm0}^{-}, \quad (18a)$$

$$\mathbf{v}_{lm2}^{-} = -i\nabla \times \mathbf{v}_{lm1}^{-}, \quad (18b)$$

and

$$\mathbf{v}_{lm1}^{+} = i\nabla \times \mathbf{v}_{lm2}^{+}, \quad (19a)$$

$$\mathbf{v}_{lm0}^{+} = i\nabla \times \mathbf{v}_{lm1}^{+}. \quad (19b)$$

The above identities imply that only the solutions \mathbf{v}_{lm0}^- and \mathbf{v}_{lm2}^+ have nonzero corresponding pressure fields, and that the solutions \mathbf{v}_{lm2}^- and \mathbf{v}_{lm0}^+ represent potential flows, i.e.,

$$\nabla \times \mathbf{v}_{lm2}^- = 0, \quad \nabla \times \mathbf{v}_{lm0}^+ = 0. \quad (20a, b)$$

The proportionality coefficient in the curl relations (18) and (19) is determined by the requirement that the expansion of the Oseen tensor in basis functions (16) and (17) has the form [37, 39]

$$\eta \mathbf{T}_0(\mathbf{r} - \mathbf{r}') = \begin{cases} \sum_{lm\sigma} \mathbf{v}_{lm\sigma}^-(\mathbf{r}) \mathbf{v}_{lm\sigma}^{+*}(\mathbf{r}'), & r > r', \\ \sum_{lm\sigma} \mathbf{v}_{lm\sigma}^+(\mathbf{r}) \mathbf{v}_{lm\sigma}^{-*}(\mathbf{r}'), & r < r'. \end{cases} \quad (21a, b)$$

The conditions (16)–(21) determine the basis fields $\mathbf{v}_{lm\sigma}^\pm$ up to a single normalization constant, which is set by an additional requirement that

$$\mathbf{v}_{lm0}^+ = \nabla r^l Y_{lm}, \quad (22)$$

where Y_{lm} is the normalized scalar spherical harmonic (as defined by Edmonds [40]).

The flow fields (16) and (17) form complete sets of singular and non-singular solutions of Stokes equations in the representation appropriate for spherical symmetry. However, they do not form orthonormal sets with respect to the natural functional scalar product for vector fields \mathbf{A} and \mathbf{B} on the spherical surface $r = b$. Following the approach of Cichocki et al. [37] we thus introduce the reciprocal basis fields $\mathbf{w}_{lm\sigma}^\pm$, which are defined by the orthogonality relations

$$\langle \delta_b^S \mathbf{w}_{lm\sigma}^\pm | \mathbf{v}_{l'm'\sigma'}^\pm \rangle = \delta_{ll'} \delta_{mm'} \delta_{\sigma\sigma'} \quad (23)$$

for all values of parameter $b > 0$, where

$$\delta_b^S(\mathbf{r}) = b^{-2} \delta(r - b), \quad (24)$$

and

$$\langle \mathbf{A} | \mathbf{B} \rangle = \int \mathbf{A}^*(\mathbf{r}) \cdot \mathbf{B}(\mathbf{r}) d\mathbf{r}. \quad (25)$$

The functions $\mathbf{w}_{lm\sigma}^\pm$ have a similar structure to the functions $\mathbf{v}_{lm\sigma}^\pm$, i.e., they have a separable form

$$\mathbf{w}_{lm\sigma}^-(\mathbf{r}) = \mathbf{W}_{lm\sigma}^-(\theta, \phi) r^{l+\sigma}, \quad (26)$$

$$\mathbf{w}_{lm\sigma}^+(\mathbf{r}) = \mathbf{W}_{lm\sigma}^+(\theta, \phi) r^{-(l+\sigma-1)}, \quad (27)$$

with the coefficients $\mathbf{W}_{lm\sigma}^\pm(\theta, \phi)$ given by combinations of vector spherical harmonics with angular order l and azimuthal order m . Explicit relations for the functions $\mathbf{V}_{lm\sigma}^\pm(\theta, \phi)$ and $\mathbf{W}_{lm\sigma}^\pm(\theta, \phi)$ in equations (16), (17), (26), and (27) are listed in Appendix A.

3.2 Equations for induced-force multipole moments

In the multipolar-representation method, the boundary-integral equation (15) is transformed into an infinite set of linear algebraic equations for the multipolar moments of the induced-force distributions (1). The multipolar expansion of the distribution \mathbf{F}_i is defined by the relation

$$\mathbf{F}_i(\mathbf{r}) = \sum_{lm\sigma} f_i(lm\sigma) \delta_a^S(\mathbf{r}_i) \mathbf{w}_{lm\sigma}^+(\mathbf{r}_i). \quad (28)$$

The corresponding multipolar moments are given by

$$\begin{aligned} f_i(lm\sigma) &= \int \mathbf{v}_{lm\sigma}^{+*}(\mathbf{r}_i) \cdot \mathbf{F}_i(\mathbf{r}) \, d\mathbf{r} \\ &= \langle \mathbf{v}_{lm\sigma}^+(i) | \mathbf{F}_i \rangle, \end{aligned} \quad (29)$$

consistent with the orthogonality relation (23). In the above equation we introduce the standard bra-ket notation, with an additional convention that $|\mathbf{A}\rangle$ represents the vector field $\mathbf{A}(\mathbf{r})$ and $|\mathbf{A}(i)\rangle$ denotes $\mathbf{A}(\mathbf{r}_i)$.

The linear algebraic equations for the multipolar moments of the induced force (29) are obtained by projecting the linear operators in the boundary-integral equation (15) onto the reciprocal basis (27). The resulting matrix representation of equation (15) can be written in the form

$$\sum_{j=1}^N \sum_{l'm'\sigma'} M_{ij}(lm\sigma | l'm'\sigma') f_j(l'm'\sigma') = c_i(lm\sigma), \quad (30)$$

where

$$M_{ij}(lm\sigma | l'm'\sigma') = Z_{ij}^{-1}(lm\sigma | l'm'\sigma') + G_{ij}^0(lm\sigma | l'm'\sigma') + G'_{ij}(lm\sigma | l'm'\sigma'), \quad (31)$$

and

$$Z_{ij}^{-1}(lm\sigma | l'm'\sigma') = \delta_{ij} \langle \delta_a^S(i) \mathbf{w}_{lm\sigma}^+(i) | \mathbf{Z}_j^{-1} | \delta_a^S(j) \mathbf{w}_{l'm'\sigma'}^+(j) \rangle, \quad (32)$$

$$G_{ij}^0(lm\sigma | l'm'\sigma') = (1 - \delta_{ij}) \langle \delta_a^S(i) \mathbf{w}_{lm\sigma}^+(i) | \mathbf{T}_0 | \delta_a^S(j) \mathbf{w}_{l'm'\sigma'}^+(j) \rangle, \quad (33)$$

$$G'_{ij}(lm\sigma | l'm'\sigma') = \langle \delta_a^S(i) \mathbf{w}_{lm\sigma}^+(i) | \mathbf{T}' | \delta_a^S(j) \mathbf{w}_{l'm'\sigma'}^+(j) \rangle. \quad (34)$$

In equations (32)–(34)

$$[\mathbf{Tb}](\mathbf{r}) = \int \mathbf{T}(\mathbf{r}, \mathbf{r}') \cdot \mathbf{b}(\mathbf{r}') d\mathbf{r}', \quad (35)$$

and the bra–ket notation introduced in equation (29) is used. The matrix elements (33) and (34) are independent of the particle radius a , because the orthogonality relation (23) holds for all values of the parameter b . The coefficients $c_i(lm\sigma)$ on the right side of equation (30) are defined by the expansion

$$\mathbf{v}_i^{\text{rb}}(\mathbf{r}) - \mathbf{v}^{\text{ext}}(\mathbf{r}) = \sum_{lm\sigma} c_i(lm\sigma) \mathbf{v}_{lm\sigma}^+(\mathbf{r}_i) \quad (36)$$

of the imposed flow field relative to the rigid-body particle motion (7) into the basis functions (17) centered at the position of particle i . Inserting the above expression into the orthogonality relation (23) yields

$$c_i(lm\sigma) = \langle \delta_a^{\text{S}}(i) \mathbf{w}_{lm\sigma}^+(i) | \mathbf{v}_i^{\text{rb}} - \mathbf{v}^{\text{ext}} \rangle. \quad (37)$$

For a system of identical particles, the matrix elements (32) of the one-particle operator \mathbf{Z}_i^{-1} are independent of the particle label i . Since the particles are assumed to be spherical, the matrix elements (32) are diagonal in the multipolar orders l and m , and independent of m ,

$$Z_{ij}^{-1}(lm\sigma | l'm'\sigma') = \delta_{ij} \delta_{ll'} \delta_{mm'} Z_i^{-1}(l; \sigma | \sigma'). \quad (38)$$

By specifying equation (30) for a single isolated particle i in an unbounded fluid and using the diagonality relation (38) we obtain the linear formula

$$\sum_{\sigma'} Z_i^{-1}(l; \sigma | \sigma') f_i(lm\sigma') = c_i(lm\sigma). \quad (39)$$

Inserting the Oseen tensor in the form (21a) into equation (11) and using the definition (29) we also get

$$\mathbf{v}_i^{\text{out}}(\mathbf{r}) = \eta^{-1} \sum_{lm\sigma} f_i(lm\sigma) \mathbf{v}_{lm\sigma}^-(\mathbf{r}_i). \quad (40)$$

According to the above relation, the multipolar moments $f_i(lm\sigma)$ can be interpreted as the expansion coefficient of the flow field $\mathbf{v}_i^{\text{out}}$ scattered by the particle i into the basis velocity fields (16). It follows that the matrix $Z_i^{-1}(l; \sigma | \sigma')$ relates the expansion coefficients of the incident and the scattered flows. For hard spheres, porous particles, spherical viscous drops, and spherical drops covered by an incompressible surfactant layer, explicit expressions for the matrix elements (38) are known [36, 37, 38]. (Note, however, a different normalization of the basis functions here and in the above references, as discussed in Appendix A)

The matrix elements of the free-space Oseen operator (33) are also known, since they are simply linked to the elements of the displacement matrix S^{+-} that was evaluated by Felderhof and Jones [41]. To show this relation we insert expression (21a), specified for $\mathbf{T}_0(\mathbf{r}_j - \mathbf{r}'_j)$ with $\mathbf{r}_j = \mathbf{r} - \mathbf{R}_j$ and $\mathbf{r}'_j = \mathbf{r}' - \mathbf{R}_j$, into equation (33), and use the orthogonality condition (23) for the fields centered at the position of the particle j . As the result we find [21]

$$G_{ij}^0(lm\sigma | l'm'\sigma') = \eta^{-1} \langle \delta_a^S(i) \mathbf{w}_{lm\sigma}^+(i) | \mathbf{v}_{l'm'\sigma'}^-(j) \rangle. \quad (41)$$

The matrix element on the right side of the above equation corresponds to the expansion of the singular flow field $\mathbf{v}_{l'm'\sigma'}^-$ centered at the position of the particle j into the nonsingular basis flow fields $\mathbf{v}_{lm\sigma}^+$ centered at the position of the particle i ,

$$\mathbf{v}_{l'm'\sigma'}^-(\mathbf{r}_j) = \sum_{lm\sigma} \mathbf{v}_{lm\sigma}^+(\mathbf{r}_i) \langle \delta_a^S(i) \mathbf{w}_{lm\sigma}^+(i) | \mathbf{v}_{l'm'\sigma'}^-(j) \rangle. \quad (42)$$

According to the definition of the displacement matrix [41] we thus have

$$G_{ij}^0(lm\sigma | l'm'\sigma') = \eta^{-1} S_S^{+-}(\mathbf{R}_i - \mathbf{R}_j; lm\sigma | l'm'\sigma'). \quad (43)$$

We note that the displacement matrix S_S^{+-} , introduced above, is normalized differently than the matrix S^{+-} defined by Felderhof and Jones [41] (cf., the transformation (A.12) between the corresponding basis fields.)

As a result of the Lorentz symmetry

$$\mathbf{T}_\alpha(\mathbf{r}, \mathbf{r}') = \mathbf{T}_\alpha^\dagger(\mathbf{r}', \mathbf{r}) \quad (44)$$

of the Green functions $\mathbf{T}_\alpha = \mathbf{T}_0, \mathbf{T}'$ (where the dagger denotes the transpose of the tensor) and the symmetry of the scalar product (25), the matrix elements (33) and (34) satisfy the reciprocal relations

$$G_{ij}^0(lm\sigma | l'm'\sigma') = G_{ji}^{0*}(l'm'\sigma' | lm\sigma), \quad (45)$$

$$G'_{ij}(lm\sigma | l'm'\sigma') = G'_{ji*}(l'm'\sigma' | lm\sigma), \quad (46)$$

where the asterisk denotes the complex conjugate. The matrix elements (38) of the one-particle scattering operator have a similar symmetry,

$$Z_i^{-1}(l; \sigma | \sigma') = Z_i^{-1}(l; \sigma' | \sigma). \quad (47)$$

The matrix elements (47) are real, due to the diagonality (38) of the matrix (32) in the azimuthal number m .

3.3 Matrix notation

In what follows we will use a compact matrix notation in the three-dimensional linear space with the components corresponding to the indices $\sigma = 0, 1, 2$ that identify the tensorial character of the basis flow fields (16) and (17). Accordingly, the matrices with the elements (32)–(34) will be denoted by $\mathbf{Z}_{ij}^{-1}(lm | l'm')$, $\mathbf{G}_{ij}^0(lm | l'm')$, and $\mathbf{G}'_{ij}(lm | l'm')$, respectively; the matrices with the elements $Z_i^{-1}(l; \sigma | \sigma')$ and $S_S^{+-}(\mathbf{R}_i - \mathbf{R}_j; lm\sigma | l'm'\sigma')$ will be denoted by $\mathbf{Z}_i^{-1}(l)$ and $\mathbf{S}_S^{+-}(\mathbf{R}_i - \mathbf{R}_j; lm | l'm')$. A similar convention will be used for three-dimensional column vectors representing quantities with a single index σ (such as the induced-force multipolar amplitudes). With this notation, equation (30) can be written in the form

$$\sum_{j=1}^N \sum_{l'm'} \mathbf{M}_{ij}(lm | l'm') \cdot \mathbf{f}_j(l'm') = \mathbf{c}_i(lm), \quad (48)$$

with the matrix \mathbf{M} given by the relation

$$\mathbf{M}_{ij}(lm | l'm') = \delta_{ij} \delta_{ll'} \delta_{mm'} \mathbf{Z}_i^{-1}(l) + \mathbf{G}_{ij}^0(lm | l'm') + \mathbf{G}'_{ij}(lm | l'm'), \quad (49)$$

according to expressions (31) and (38). In the above equations, $\mathbf{f}_i(lm)$ and $\mathbf{c}_i(lm)$ are column vectors with components $f_i(lm\sigma)$ and $c_i(lm\sigma)$, and the dot represents the matrix multiplication.

An analogous matrix notation will be used in the Cartesian representation, which is introduced in the following section.

4 Cartesian basis

Using the force-multipole equations (48) to determine the hydrodynamic friction matrix in a suspension bounded by planar walls involves evaluation of the spherical matrix elements (34) of the Green function $\mathbf{T}'(\mathbf{r}, \mathbf{r}')$ that describes the flow field in the bounded domain. For a single wall the matrix elements were calculated by Cichocki et al. [20, 21] using a multipolar-image representation of the flow reflected from a planar boundary. For a suspension confined between two parallel walls, the matrix elements (34) can be evaluated using the image representation derived by Bhattacharya and Blawdziewicz [27]; however such calculations are inefficient due to convergence problems. Here we propose an alternative approach, in which the matrix elements (48) are determined by means of Cartesian representation of the flow fields, consistent with the wall geometry.

In what follows we assume that the walls are normal to the axis z in the Cartesian coordinate system (x, y, z) . The corresponding Cartesian unit vectors are denoted $\hat{\mathbf{e}}_x, \hat{\mathbf{e}}_y, \hat{\mathbf{e}}_z$.

4.1 Definition of Cartesian basis flow fields

We introduce two basis sets of Stokes flows $\mathbf{v}_{\mathbf{k}\sigma}^-$ and $\mathbf{v}_{\mathbf{k}\sigma}^+$, defined by the expressions

$$\mathbf{v}_{\mathbf{k}0}^-(\mathbf{r}) = (32\pi^2)^{-1/2} \left[i(1 - 2kz)\hat{\mathbf{k}} + (1 + 2kz)\hat{\mathbf{e}}_z \right] k^{-1/2} e^{i\mathbf{k} \cdot \boldsymbol{\rho} - kz}, \quad (50a)$$

$$\mathbf{v}_{\mathbf{k}1}^-(\mathbf{r}) = (8\pi^2)^{-1/2} (\hat{\mathbf{k}} \times \hat{\mathbf{e}}_z) k^{-1/2} e^{i\mathbf{k} \cdot \boldsymbol{\rho} - kz}, \quad (50b)$$

$$\mathbf{v}_{\mathbf{k}2}^-(\mathbf{r}) = (32\pi^2)^{-1/2} (i\hat{\mathbf{k}} - \hat{\mathbf{e}}_z) k^{-1/2} e^{i\mathbf{k} \cdot \boldsymbol{\rho} - kz}, \quad (50c)$$

and

$$\mathbf{v}_{\mathbf{k}0}^+(\mathbf{r}) = (32\pi^2)^{-1/2} (i\hat{\mathbf{k}} + \hat{\mathbf{e}}_z) k^{-1/2} e^{i\mathbf{k} \cdot \boldsymbol{\rho} + kz}, \quad (51a)$$

$$\mathbf{v}_{\mathbf{k}1}^+(\mathbf{r}) = (8\pi^2)^{-1/2} (\hat{\mathbf{k}} \times \hat{\mathbf{e}}_z) k^{-1/2} e^{i\mathbf{k} \cdot \boldsymbol{\rho} + kz}, \quad (51b)$$

$$\mathbf{v}_{\mathbf{k}2}^+(\mathbf{r}) = (32\pi^2)^{-1/2} \left[i(1 + 2kz)\hat{\mathbf{k}} - (1 - 2kz)\hat{\mathbf{e}}_z \right] k^{-1/2} e^{i\mathbf{k} \cdot \boldsymbol{\rho} + kz}. \quad (51c)$$

The pressure fields corresponding to the flows (50) and (51) are

$$p_{\mathbf{k}0}^-(\mathbf{r}) = (2\pi^2)^{-1/2} \eta k^{1/2} e^{i\mathbf{k} \cdot \boldsymbol{\rho} - kz}, \quad p_{\mathbf{k}2}^-(\mathbf{r}) = (2\pi^2)^{-1/2} \eta k^{1/2} e^{i\mathbf{k} \cdot \boldsymbol{\rho} - kz}, \quad (52)$$

and

$$p_{\mathbf{k}1}^-(\mathbf{r}) = p_{\mathbf{k}2}^-(\mathbf{r}) = p_{\mathbf{k}0}^+(\mathbf{r}) = p_{\mathbf{k}1}^+(\mathbf{r}) = 0. \quad (53)$$

In the above relations

$$\boldsymbol{\rho} = x\hat{\mathbf{e}}_x + y\hat{\mathbf{e}}_y \quad (54)$$

is the projection of the vector \mathbf{r} onto the x - y plane, and

$$\mathbf{k} = k_x\hat{\mathbf{e}}_x + k_y\hat{\mathbf{e}}_y \quad (55)$$

is the corresponding two-dimensional wave vector. Furthermore, $\hat{\mathbf{k}} = \mathbf{k}/k$ and $k = |\mathbf{k}|$.

The basis sets (50) and (51) are determined by the following conditions: Firstly, each basis flow field $\mathbf{v}_{\mathbf{k}\sigma}^\pm$ corresponds to a single lateral Fourier mode; secondly, the velocity fields $\mathbf{v}_{\mathbf{k}\sigma}^-(\mathbf{r})$ vanish for $z \rightarrow \infty$ and $\mathbf{v}_{\mathbf{k}\sigma}^+(\mathbf{r})$ for $z \rightarrow -\infty$; thirdly,

the basis fields $\mathbf{v}_{\mathbf{k}\sigma}^+$ are obtained from $\mathbf{v}_{\mathbf{k}2-\sigma}^-$ by reflection with respect to the plane x - y . The fourth condition is the set of curl relations

$$\mathbf{v}_{\mathbf{k}1}^- = -\frac{1}{2}ik^{-1}\nabla \times \mathbf{v}_{\mathbf{k}0}^-, \quad (56a)$$

$$\mathbf{v}_{\mathbf{k}2}^- = -\frac{1}{2}ik^{-1}\nabla \times \mathbf{v}_{\mathbf{k}1}^-, \quad (56b)$$

and

$$\mathbf{v}_{\mathbf{k}1}^+ = \frac{1}{2}ik^{-1}\nabla \times \mathbf{v}_{\mathbf{k}2}^+, \quad (57a)$$

$$\mathbf{v}_{\mathbf{k}0}^+ = \frac{1}{2}ik^{-1}\nabla \times \mathbf{v}_{\mathbf{k}1}^+, \quad (57b)$$

by analogy to the expressions (18)–(20) for the spherical basis. Relations (56) and (57) imply

$$\nabla \times \mathbf{v}_{\mathbf{k}2}^- = 0, \quad \nabla \times \mathbf{v}_{\mathbf{k}0}^+ = 0. \quad (58a, b)$$

The final condition is the requirement that the basis fields (50) and (51) satisfy the identity

$$\eta \mathbf{T}_0(\mathbf{r} - \mathbf{r}') = \begin{cases} \int_{\mathbf{k}} d\mathbf{k} \sum_{\sigma} \mathbf{v}_{\mathbf{k}\sigma}^-(\mathbf{r}) \mathbf{v}_{\mathbf{k}\sigma}^{+*}(\mathbf{r}'), & z > z', \\ \int_{\mathbf{k}} d\mathbf{k} \sum_{\sigma} \mathbf{v}_{\mathbf{k}\sigma}^+(\mathbf{r}) \mathbf{v}_{\mathbf{k}\sigma}^{-*}(\mathbf{r}'), & z < z', \end{cases} \quad (59a, b)$$

where the integration is over the two-dimensional Fourier space (55). The identity (59) is analogous to the representation (21) of the Oseen tensor in the spherical basis. It can be verified by showing that

$$\mathbf{v}_{\mathbf{k}\sigma}^{\mp}(\mathbf{r}) \mathbf{v}_{\mathbf{k}\sigma}^{\pm*}(\mathbf{r}') = \eta \hat{\mathbf{T}}_0(\mathbf{k}, z - z') e^{i\mathbf{k} \cdot (\boldsymbol{\rho} - \boldsymbol{\rho}'),} \quad (60)$$

where

$$\eta \hat{\mathbf{T}}_0(\mathbf{k}, z) = \frac{1}{16\pi^2} [2\hat{\mathbf{I}} - (1 + k|z|)\hat{\mathbf{k}}\hat{\mathbf{k}} - ikz(\hat{\mathbf{k}}\hat{\mathbf{e}}_z + \hat{\mathbf{e}}_z\hat{\mathbf{k}}) - (1 - k|z|)\hat{\mathbf{e}}_z\hat{\mathbf{e}}_z] k^{-1} e^{-k|z|}, \quad (61)$$

is the two-dimensional Fourier transform in the x - y plane of the Oseen tensor,

$$\hat{\mathbf{T}}_0(\mathbf{k}, z) = \frac{1}{(2\pi)^2} \int \mathbf{T}_0(\mathbf{r}) e^{-i\mathbf{k} \cdot \boldsymbol{\rho}} d\boldsymbol{\rho}. \quad (62)$$

The reciprocal sets of vector fields $\mathbf{w}_{\mathbf{k}\sigma}^{\pm}$ that correspond to the Cartesian basis sets $\mathbf{v}_{\mathbf{k}\sigma}^{\pm}$ are defined by the orthogonality relations

$$\langle \delta_h^C \mathbf{w}_{\mathbf{k}\sigma}^{\pm} | \mathbf{v}_{\mathbf{k}'\sigma'}^{\pm} \rangle = \delta(\mathbf{k} - \mathbf{k}') \delta_{\sigma\sigma'}, \quad (63)$$

which hold for all values of the parameter h , where

$$\delta_h^C(\mathbf{r}) = \delta(z - h). \quad (64)$$

Inserting expressions (50) and (51) into the above relations yields

$$\mathbf{w}_{\mathbf{k}0}^{\pm}(\mathbf{r}) = 4k\mathbf{v}_{\mathbf{k}0}^{\mp}(\mathbf{r}), \quad \mathbf{w}_{\mathbf{k}1}^{\pm}(\mathbf{r}) = 2k\mathbf{v}_{\mathbf{k}1}^{\mp}(\mathbf{r}), \quad \mathbf{w}_{\mathbf{k}2}^{\pm}(\mathbf{r}) = 4k\mathbf{v}_{\mathbf{k}2}^{\mp}(\mathbf{r}). \quad (65)$$

4.2 Displacement theorem for Cartesian basis

The Cartesian basis fields (50) and (51) centered at different points \mathbf{R}_1 and \mathbf{R}_2 are related by simple displacement transformations. Due to the translational invariance, the transformations are diagonal in the wave vector \mathbf{k} ,

$$\mathbf{v}_{\mathbf{k}\sigma}^{-}(\mathbf{r}_2) = \sum_{\sigma'} \mathbf{v}_{\mathbf{k}\sigma'}^{-}(\mathbf{r}_1) S_C^{-}(\mathbf{R}_{12}, \mathbf{k}; \sigma' | \sigma), \quad (66a)$$

$$\mathbf{v}_{\mathbf{k}\sigma}^{+}(\mathbf{r}_2) = \sum_{\sigma'} \mathbf{v}_{\mathbf{k}\sigma'}^{+}(\mathbf{r}_1) S_C^{+}(\mathbf{R}_{12}, \mathbf{k}; \sigma' | \sigma), \quad (66b)$$

where $\mathbf{r}_1 = \mathbf{r} - \mathbf{R}_1$, $\mathbf{r}_2 = \mathbf{r} - \mathbf{R}_2$, and $\mathbf{R}_{12} = \mathbf{R}_1 - \mathbf{R}_2$. Using the orthogonality condition (63) and the completeness of the Cartesian basis sets we get

$$\langle \delta_0^C(1) \mathbf{w}_{\mathbf{k}'\sigma'}^{\pm}(1) | \mathbf{v}_{\mathbf{k}\sigma}^{\pm}(2) \rangle = \delta(\mathbf{k} - \mathbf{k}') S_C^{\pm\pm}(\mathbf{R}_{12}, \mathbf{k}; \sigma' | \sigma). \quad (67)$$

Relations (66) and the expression (67) for the elements $S_C^{\pm\pm}(\mathbf{R}_{12}, \mathbf{k}; \sigma' | \sigma)$ of the Cartesian displacement matrix $\mathbf{S}_C^{\pm\pm}(\mathbf{R}_{12}, \mathbf{k})$ are analogous to the displacement formulas (41)–(43) for the spherical basis fields.

An analysis of equations (50) and (51) indicates that the matrices $\mathbf{S}_C^{\pm\pm}(\mathbf{R}_{12}, \mathbf{k})$ can be written in the factorized form

$$\mathbf{S}_C^{\pm\pm}(\mathbf{R}_{12}, \mathbf{k}) = \tilde{\mathbf{S}}_C^{\pm\pm}(kZ_{12}) e^{i\mathbf{k} \cdot \boldsymbol{\rho}_{12}}, \quad (68)$$

where

$$\mathbf{R}_{12} = \boldsymbol{\rho}_{12} + Z_{12}\hat{\mathbf{e}}_z, \quad (69)$$

and

$$\tilde{\mathbf{S}}_C^{-}(kZ) = \begin{bmatrix} 1 & 0 & 0 \\ 0 & 1 & 0 \\ -2kZ & 0 & 1 \end{bmatrix} \mathbf{e}^{-kZ}, \quad \tilde{\mathbf{S}}_C^{+}(kZ) = \begin{bmatrix} 1 & 0 & 2kZ \\ 0 & 1 & 0 \\ 0 & 0 & 1 \end{bmatrix} \mathbf{e}^{kZ}. \quad (70)$$

It is also easy to verify that the matrices $\mathbf{S}_C^{\pm\pm}$ obey the group property

$$\mathbf{S}_C^{\pm\pm}(\mathbf{R} + \mathbf{R}', \mathbf{k}) = \mathbf{S}_C^{\pm\pm}(\mathbf{R}, \mathbf{k}) \cdot \mathbf{S}_C^{\pm\pm}(\mathbf{R}', \mathbf{k}) \quad (71)$$

with

$$\mathbf{S}_C^{\pm\pm}(0, \mathbf{k}) = \hat{\mathbf{I}}, \quad (72)$$

and that they satisfy the symmetry relation

$$\mathbf{S}_C^{++}(\mathbf{R}, \mathbf{k}) = [\mathbf{S}_C^{--}(-\mathbf{R}, \mathbf{k})]^\dagger, \quad (73)$$

where the dagger denotes the Hermitian conjugate.

4.3 Transformations between Cartesian and spherical basis sets

One of the key results of our study is a set of transformation relations between the spherical basis fields (16) and (17) and the Cartesian basis fields (50) and (51). We focus on the transformations

$$\mathbf{v}_{lm\sigma}^-(\mathbf{r}_2) = \int d\mathbf{k}' \sum_{\sigma'} \mathbf{v}_{\mathbf{k}'\sigma'}^\pm(\mathbf{r}_1) \langle \delta_0^C(1) \mathbf{w}_{\mathbf{k}'\sigma'}^\pm(1) | \mathbf{v}_{lm\sigma}^-(2) \rangle \quad (74)$$

and

$$\mathbf{v}_{\mathbf{k}\sigma}^\pm(\mathbf{r}_2) = \sum_{l'm'\sigma'} \mathbf{v}_{l'm'\sigma'}^\pm(\mathbf{r}_1) \langle \delta_a^S(1) \mathbf{w}_{l'm'\sigma'}^\pm(1) | \mathbf{v}_{\mathbf{k}\sigma}^\pm(2) \rangle \quad (75)$$

that are needed for evaluating the spherical matrix elements (34) of the Green function representing the flow scattered from the walls.

Recalling notation (2) and definition (16) we note that the basis fields $\mathbf{v}_{lm\sigma}^-(\mathbf{r}_2)$ are singular at $\mathbf{r} = \mathbf{R}_2$. Accordingly, the transformation formula (74) is valid for $\pm(\mathbf{R}_2 - \mathbf{R}_1) \cdot \hat{\mathbf{e}}_z > 0$. We also note that the integral defining the matrix element on the right side of (74) is not absolutely convergent for $l + \sigma \leq 2$, because of the slow convergence of the field (16) at infinity; the principal-value interpretation of the integral is employed in this case.

Using the Cartesian displacement relations (66), the matrix elements on the right side of equations (74) and (75) can be factorized into the products of the displacement matrices (68) and the position-independent matrices $\mathbf{T}_{CS}^{\pm-}(\mathbf{k}, lm)$ and $\mathbf{T}_{SC}^{+\pm}(lm, \mathbf{k})$,

$$\langle \delta_0^C(1) \mathbf{w}_{\mathbf{k}\sigma}^\pm(1) | \mathbf{v}_{l'm'\sigma'}^\pm(2) \rangle = [\mathbf{S}_C^{\pm\pm}(\mathbf{R}_{12}, \mathbf{k}) \cdot \mathbf{T}_{CS}^{\pm-}(\mathbf{k}, l'm')]_{\sigma\sigma'}, \quad (76)$$

$$\langle \delta_a^S(1) \mathbf{w}_{lm\sigma}^\pm(1) | \mathbf{v}_{\mathbf{k}'\sigma'}^\pm(2) \rangle = [\mathbf{T}_{SC}^{+\pm}(lm, \mathbf{k}') \cdot \mathbf{S}_C^{\pm\pm}(\mathbf{R}_{12}, \mathbf{k}')]_{\sigma\sigma'}. \quad (77)$$

Equation (68) indicates that the matrix element (76) is nonsingular in the limit $\mathbf{R}_{12} \rightarrow 0$, even though the integrand in the scalar product is singular at $\mathbf{r} = 0$ for $\mathbf{R}_1 = \mathbf{R}_2$. (In contrast, relation (77) does not involve any singular integrals.) In the limit $\mathbf{R}_{12} \rightarrow 0$, equations (72) and (74)–(77) yield the transformation relations

$$\mathbf{v}_{lm\sigma}^-(\mathbf{r}) = \int d\mathbf{k}' \sum_{\sigma'} \mathbf{v}_{\mathbf{k}'\sigma'}^\pm(\mathbf{r}) T_{CS}^{\pm-}(\mathbf{k}', lm; \sigma' | \sigma), \quad \pm z < 0, \quad (78)$$

$$\mathbf{v}_{\mathbf{k}\sigma}^{\pm}(\mathbf{r}) = \sum_{l'm'\sigma'} \mathbf{v}_{l'm'\sigma'}^{\pm}(\mathbf{r}) T_{\text{SC}}^{\pm\pm}(l'm', \mathbf{k}; \sigma' | \sigma). \quad (79)$$

The matrices $\mathbf{T}_{\text{CS}}^{\pm-}(\mathbf{k}, lm)$ and $\mathbf{T}_{\text{SC}}^{\pm\pm}(lm, \mathbf{k})$ have several important symmetries. First, we recall that the Cartesian basis sets (50) and (51) are related to each other via the reflection with respect to the plane $z = 0$. The corresponding symmetries of the transformation matrices are

$$\mathbf{T}_{\text{CS}}^{--}(\mathbf{k}, lm; \sigma | \sigma') = (-1)^{l+m+\sigma'} \mathbf{T}_{\text{CS}}^{+-}(\mathbf{k}, lm; 2 - \sigma | \sigma'), \quad (80)$$

$$\mathbf{T}_{\text{SC}}^{+-}(lm, \mathbf{k}; \sigma | \sigma') = (-1)^{l+m+\sigma} \mathbf{T}_{\text{SC}}^{++}(lm, \mathbf{k}; \sigma | 2 - \sigma'). \quad (81)$$

Another important symmetry relation is associated with the representations (21) and (59) of the Oseen tensor in the spherical and Cartesian bases. The relation is obtained by applying the Oseen integral operator with the kernel in the respective forms (21b) and (59) to the fields $\mathbf{w}_{\mathbf{k}\sigma}^{\pm}$, which yields

$$\int \mathbf{T}_0(\mathbf{r}_1 - \mathbf{r}'_1) \delta_0^{\text{C}}(\mathbf{r}'_2) \mathbf{w}_{\mathbf{k}\sigma}^{\pm}(\mathbf{r}'_2) d\mathbf{r}' = \sum_{l'm'\sigma'} \mathbf{v}_{l'm'\sigma'}^{\pm}(\mathbf{r}_1) \langle \mathbf{v}_{l'm'\sigma'}^{\pm}(1) | \delta_0^{\text{C}}(2) \mathbf{w}_{\mathbf{k}\sigma}^{\pm}(2) \rangle \quad (82)$$

and

$$\int \mathbf{T}_0(\mathbf{r}_1 - \mathbf{r}'_1) \delta_0^{\text{C}}(\mathbf{r}'_2) \mathbf{w}_{\mathbf{k}\sigma}^{\pm}(\mathbf{r}'_2) d\mathbf{r}' = \int d\mathbf{k}' \sum_{\sigma'} \mathbf{v}_{\mathbf{k}'\sigma'}^{\mp}(\mathbf{r}_1) \langle \mathbf{v}_{\mathbf{k}'\sigma'}^{\pm}(1) | \delta_0^{\text{C}}(2) \mathbf{w}_{\mathbf{k}\sigma}^{\pm}(2) \rangle. \quad (83)$$

By comparing the above expressions in the limit $\mathbf{R}_{12} \rightarrow 0$ we find

$$\mathbf{v}_{\mathbf{k}\sigma}^{\mp}(\mathbf{r}) = \sum_{l'm'\sigma'} \mathbf{v}_{l'm'\sigma'}^{\pm}(\mathbf{r}) T_{\text{CS}}^{\pm- *}(\mathbf{k}, lm; \sigma | \sigma'), \quad (84)$$

where equations (72) and (76) and the orthogonality condition (63) were applied. Since the expansion of the flow fields $\mathbf{v}_{\mathbf{k}\sigma}^{\pm}(\mathbf{r})$ into $\mathbf{v}_{l'm'\sigma'}^{\pm}(\mathbf{r})$ is unique, equations (79) and (84) imply the symmetry

$$\mathbf{T}_{\text{SC}}^{+\mp}(lm, \mathbf{k}) = [\mathbf{T}_{\text{CS}}^{\pm-}(\mathbf{k}, lm)]^{\dagger}. \quad (85)$$

The functional dependence of the matrices $\mathbf{T}_{\text{SC}}^{\pm\pm}$ and $\mathbf{T}_{\text{CS}}^{\pm-}$ on the wave vector \mathbf{k} can also be derived using symmetry considerations. Specifically, one can show that

$$T_{\text{SC}}^{\pm\pm}(lm, \mathbf{k}; \sigma | \sigma') \sim k^{-1/2} k^{l+\sigma-1} e^{im\psi}, \quad (86a)$$

$$T_{\text{CS}}^{\pm-}(\mathbf{k}, lm; \sigma | \sigma') \sim k^{-1/2} k^{l+\sigma'-1} e^{-im\psi}, \quad (86b)$$

where $\mathbf{k} = (k, \psi)$ is the representation of the wave vector in the polar coordinates. The angular form of relations (86) stems from the requirement in the definition of the basis fields (16) and (17) that the coefficients $\mathbf{V}_{lm\sigma}^{\pm}(\theta, \phi)$ are combinations of spherical harmonics of order m . The dependence on the amplitude of the wave vector k results from the invariance of the transformation relations (78) and (79) with respect to the scale change

$$\mathbf{r} \rightarrow \alpha \mathbf{r}, \quad \mathbf{k} \rightarrow \alpha^{-1} \mathbf{k}, \quad (87)$$

where α is a real parameter (cf., expressions (16), (17) and (50), (51) for the spherical and Cartesian basis fields). Using equations (86), the matrices $\mathbf{T}_{\text{SC}}^{+\pm}(lm, \mathbf{k})$ and $\mathbf{T}_{\text{CS}}^{\pm-}(\mathbf{k}, lm)$ can be represented in the factorized form

$$\mathbf{T}_{\text{SC}}^{+\pm}(lm, \mathbf{k}) = (-i)^m (2\pi k)^{-1/2} e^{-im\psi} \mathbf{K}(k, l) \cdot \tilde{\mathbf{T}}_{\text{SC}}^{+\pm}(lm), \quad (88a)$$

$$\mathbf{T}_{\text{CS}}^{\pm-}(\mathbf{k}, lm) = i^m (2\pi k)^{-1/2} e^{im\psi} \tilde{\mathbf{T}}_{\text{CS}}^{\pm-}(lm) \cdot \mathbf{K}(k, l), \quad (88b)$$

where $\mathbf{K}(k, l)$ is a diagonal matrix with the elements

$$K(k, l; \sigma \mid \sigma') = \delta_{\sigma\sigma'} k^{l+\sigma-1}. \quad (89)$$

A further simplification of the structure of the transformation matrices $\mathbf{T}_{\text{SC}}^{+\pm}$ and $\mathbf{T}_{\text{CS}}^{\pm-}$ results from the curl relations (18)–(20) and (56)–(58). By taking curl of both sides of equations (78) and (79), applying the symmetries (80), (81), and (85), and using the factorization formulas (88), one can show that the matrices $\tilde{\mathbf{T}}_{\text{SC}}^{+\pm}(lm)$ and $\tilde{\mathbf{T}}_{\text{CS}}^{\pm-}(lm)$ have the following triangular structure

$$\tilde{\mathbf{T}}_{\text{SC}}^{++} = \begin{bmatrix} a & b & c \\ 0 & 2a & 2b \\ 0 & 0 & 4a \end{bmatrix}, \quad \tilde{\mathbf{T}}_{\text{SC}}^{+-} = (-1)^{l+m} \begin{bmatrix} c & b & a \\ -2b & -2a & 0 \\ 4a & 0 & 0 \end{bmatrix}, \quad (90a)$$

$$\tilde{\mathbf{T}}_{\text{CS}}^{+-} = (-1)^{l+m} \begin{bmatrix} c & -2b & 4a \\ b & -2a & 0 \\ a & 0 & 0 \end{bmatrix}, \quad \tilde{\mathbf{T}}_{\text{CS}}^{--} = \begin{bmatrix} a & 0 & 0 \\ b & 2a & 0 \\ c & 2b & 4a \end{bmatrix}, \quad (90b)$$

and involve only three independent coefficients. As shown in Appendix C, the expressions for the coefficients a, b, c are

$$a = [4(l-m)!(l+m)!(2l+1)]^{-1/2}, \quad (91a)$$

$$b = 2am/l, \quad (91b)$$

$$c = a \frac{l(2l^2 - 2l - 1) - 2m^2(l-2)}{l(2l-1)}. \quad (91c)$$

Relations (68)–(73) and (88)–(91) represent the key results of the analysis presented so far. In Section 5 we apply these results to express the spherical matrix elements of the free-space Green operator (33) in terms of two-dimensional Fourier integrals (which can be explicitly evaluated in this case). The Fourier representations of matrix elements (34) for a system bounded by a single planar wall and by two parallel planar walls are derived in §6 and §7, respectively. These results enable efficient numerical evaluation of the multiparticle friction matrix in wall-bounded suspensions. Description of our algorithm is given in Section 8, and examples of numerical results are shown in Section 9.

5 Fourier representation of the spherical displacement matrix

In this section we apply the Cartesian displacement formulas (70) and transformation matrices (88)–(90) to express the spherical displacement matrix \mathbf{S}_s^{+-} in terms of two-dimensional Fourier integrals. Such a representation can be utilized in developing numerical algorithms for evaluating hydrodynamic interactions in doubly periodic systems. Moreover, the analysis allows us to introduce some techniques that will be used in the discussion of the flow in wall-bounded suspensions (cf. Sections 6 and 7).

We recall that the displacement matrix \mathbf{S}_s^{+-} and the corresponding spherical matrix elements (33) of the Oseen operator are equivalent, as indicated by the formula (43). To make the notation in this and the following sections parallel, we express our results in terms of the matrix elements $\mathbf{G}_{ij}^0(lm | l'm')$.

By inserting the expansion (78) into (41) and using equation (77) we find

$$\mathbf{G}_{ij}^0(lm | l'm') = \eta^{-1} \int d\mathbf{k} \, \mathbf{T}_{SC}^{+\pm}(lm, \mathbf{k}) \cdot \mathbf{S}_C^{\pm\pm}(\mathbf{R}_{ij}, \mathbf{k}) \cdot \mathbf{T}_{CS}^{\pm-}(\mathbf{k}, l'm'), \quad (92)$$

where the plus sign applies for $\mathbf{R}_{ij} \cdot \hat{\mathbf{e}}_z < 0$ and the minus sign for $\mathbf{R}_{ij} \cdot \hat{\mathbf{e}}_z > 0$. We note that the Lorentz symmetry (45) of the matrix elements $\mathbf{G}_{ij}^0(lm | l'm')$ is explicit in equation (92) due to the symmetry relations (73) and (85) for the component matrices. The angular integration in relation (92) can be explicitly performed with a help of the factorization formulas (68) and (88) and the

equation

$$\int_0^{2\pi} e^{i(k\rho \cos \psi - m\psi)} d\psi = 2\pi i^m J_m(k\rho), \quad (93)$$

where $J_m(x)$ is the Bessel function of the order m . The resulting expression has the form

$$\begin{aligned} G_{ij}^0(lm\sigma | l'm'\sigma') &= \eta^{-1}(-1)^{m'-m} e^{i(m'-m)\phi_{ij}} \\ &\times \int_0^\infty g_0^\pm(kZ_{ij}; lm\sigma | l'm'\sigma') k^{l+l'+\sigma+\sigma'-2} J_{m-m'}(k\rho_{ij}) dk, \end{aligned} \quad (94)$$

where $(\rho_{ij}, \phi_{ij}, Z_{ij})$ is the representation of the vector \mathbf{R}_{ij} in the cylindrical coordinates, and

$$\mathbf{g}_0^\pm(kz; lm | l'm') = \tilde{\mathbf{T}}_{SC}^{+\pm}(lm) \cdot \tilde{\mathbf{S}}_C^{\pm\pm}(kz) \cdot \tilde{\mathbf{T}}_{CS}^{\pm-}(l'm'). \quad (95)$$

Relations (70) and (95) indicate that the integrand in equation (94) is a combination of the Bessel function, powers of k , and the exponential $e^{-k|Z_{ij}|}$. The integrals of this form can be evaluated using the following identity

$$\int_0^\infty k^l J_m(k\rho) e^{-kz} dk = (-1)^m (l-m)! r^{-(l+1)} P_l^m(r^{-1}z), \quad z > 0, \quad (96)$$

where $P_l^m(x)$ is the associated Legendre polynomial, and

$$r = (\rho^2 + z^2)^{1/2}. \quad (97)$$

We have verified that equations (94)–(96) yield expressions that are equivalent to the displacement theorems for the spherical basis of Stokes flows derived by Felderhof and Jones [41]. In development of the multipolar-expansion algorithms to evaluate hydrodynamic interactions in doubly-periodic systems, a direct application of the Fourier representation (92) may be useful.

6 Single-wall Green operator

Similar techniques can be used to evaluate the matrix elements of the Green operator (34) in a system bounded by a single planar wall. We assume that the wall is in the plane

$$z = Z_w \quad (98)$$

and the suspension occupies either the halfspace $z > Z_w$ (denoted by Ω^+) or $z < Z_w$ (denoted by Ω^-). The spherical matrix elements of the Green operator (34) for this system are obtained by combining the transformation relations (88)–(90) between the spherical and Cartesian basis sets with the Cartesian representation of the flow reflected from the wall. The reflected flow is discussed in the following subsection.

6.1 Single-wall reflection matrix

The velocity field in the halfspace Ω^\pm , occupied by the fluid, can be uniquely decomposed into the incoming and reflected flows

$$\mathbf{v}(\mathbf{r}) = \mathbf{v}_w^{\text{in}}(\mathbf{r}) + \mathbf{v}_w^{\text{out}}(\mathbf{r}), \quad (99)$$

where

$$\mathbf{v}_w^{\text{in}}(\mathbf{r}) = \int d\mathbf{k} \sum_{\sigma} c_w^{\text{in}}(\mathbf{k}\sigma) \mathbf{v}_{\mathbf{k}\sigma}^{\pm}(\mathbf{r}_w), \quad (100a)$$

$$\mathbf{v}_w^{\text{out}}(\mathbf{r}) = \int d\mathbf{k} \sum_{\sigma} c_w^{\text{out}}(\mathbf{k}\sigma) \mathbf{v}_{\mathbf{k}\sigma}^{\mp}(\mathbf{r}_w). \quad (100b)$$

In the above relations

$$\mathbf{r}_w = \mathbf{r} - \mathbf{R}_w \quad (101)$$

denotes the position of the point \mathbf{r} relative to the wall, where $\mathbf{R}_w = (X_w, Y_w, Z_w)$ has arbitrary lateral coordinates X_w and Y_w .

According to the definitions (50) and (51), the decay of the basis flow fields $\mathbf{v}_{\mathbf{k}\sigma}^{\mp}(\mathbf{r}_w)$ for $k \rightarrow \infty$ is faster in the halfspace Ω^\pm than it is on the wall surface (98). Thus, assuming that the integral (100b) converges on the surface (98), the scattered flow field $\mathbf{v}_w^{\text{out}}(\mathbf{r})$ is nonsingular in the whole region Ω^\pm occupied by the fluid. Likewise, the convergence of the integral (100a) on the wall surface implies that the incoming flow field $\mathbf{v}_w^{\text{in}}(\mathbf{r})$ is nonsingular in the complementary region Ω^\mp .

By analogy with the relations (39) and (40) for a flow field scattered by a particle, we introduce the single-wall scattering matrix \mathbf{Z}_w , defined by the equation

$$\mathbf{c}_w^{\text{out}}(\mathbf{k}) = -\mathbf{Z}_w \cdot \mathbf{c}_w^{\text{in}}(\mathbf{k}), \quad (102)$$

where $\mathbf{c}_w^{\text{out}}(\mathbf{k})$ and $\mathbf{c}_w^{\text{in}}(\mathbf{k})$ denote the arrays of expansion coefficients in equations (100). For an immobile rigid wall, the velocity field (99) vanishes at $z = Z_w$. By inspection of expressions (50) and (51) we find that

$$\mathbf{Z}_w = \begin{bmatrix} 1 & 0 & 0 \\ 0 & 1 & 0 \\ 0 & 0 & 1 \end{bmatrix} \quad (103)$$

in this case. For planar interfaces with other boundary conditions (e.g., a surfactant-covered fluid-fluid interface discussed in [42]) the scattering matrix is different from identity, and it may depend on the magnitude of the wave vector k . Explicit expressions for scattering matrices for such systems will be derived in forthcoming publications.

6.2 Matrix elements of Green operator

In order to evaluate matrix elements (34) of the single-wall Green operator we consider the flow field produced by the induced-force distribution (1) centered at the position of particle j . By comparing the decompositions (4) and (99) and using relation (78) we find

$$\mathbf{v}_w^{\text{in}}(\mathbf{r}) = \int \mathbf{T}_0(\mathbf{r} - \mathbf{r}') \cdot \mathbf{F}_j(\mathbf{r}') d\mathbf{r}' \quad (104)$$

and

$$\mathbf{v}_w^{\text{out}}(\mathbf{r}) = \int \mathbf{T}'(\mathbf{r}, \mathbf{r}') \cdot \mathbf{F}_j(\mathbf{r}') d\mathbf{r}'. \quad (105)$$

We note that according to equations (11) and (104) the flow incident to the wall equals to the flow scattered by the particle

$$\mathbf{v}_w^{\text{in}}(\mathbf{r}) = \mathbf{v}_j^{\text{out}}(\mathbf{r}). \quad (106)$$

By projecting equation (105) onto the reciprocal spherical basis $\mathbf{w}_{lm\sigma}^+$ centered at the position of particle i and using the multipolar expansion (29) we get

$$\langle \delta_a^S(i) \mathbf{w}_{lm\sigma}^+(i) | \mathbf{v}_w^{\text{out}} \rangle = \sum_{l'm'\sigma'} G'_{ij}(lm\sigma | l'm'\sigma') f_j(l'm'\sigma'), \quad (107)$$

where the definition (34) was applied. The matrix element of the reflected flow at the left side of the above equation is evaluated with the help of the reflection relation (102). Accordingly, the expansion coefficients of the incoming flow

$$c_w^{\text{in}}(\mathbf{k}\sigma) = \langle \delta_0^C(w) \mathbf{w}_{\mathbf{k}\sigma}^\pm(w) | \mathbf{v}_w^{\text{in}} \rangle \quad (108)$$

(where the index w in the bra $\langle \delta_0^C(w) \mathbf{w}_{\mathbf{k}\sigma}^\pm(w) |$ indicates the dependence on the variable (101)) are determined using expansion (40) for the incoming velocity field (106) and the relation (76) for the matrix elements relating the spherical and reciprocal basis fields. Collecting these formulas yields

$$\mathbf{c}_w^{\text{in}}(\mathbf{k}) = \eta^{-1} \sum_{l'm'} \mathbf{S}_C^{\pm\pm}(\mathbf{R}_{wj}, \mathbf{k}) \cdot \mathbf{T}_{CS}^{\pm-}(\mathbf{k}, l'm') \cdot \mathbf{f}_j(l'm'), \quad (109)$$

where $\mathbf{R}_{iw} = \mathbf{R}_i - \mathbf{R}_w$ and $\mathbf{R}_{wj} = \mathbf{R}_w - \mathbf{R}_j$. The above relation is combined with the expansion (100b) and the scattering formula (102); the resulting expression for $\mathbf{v}_w^{\text{out}}$ is inserted into (107). The matrix elements between the spherical and Cartesian basis fields are then evaluated using (77). By comparing the result of this calculation to the expression (107) we find

$$\mathbf{G}'_{ij}(lm | l'm') = -\eta^{-1} \int d\mathbf{k} \mathbf{T}_{SC}^{+\mp}(lm, \mathbf{k}) \cdot \mathbf{S}_C^{\mp\mp}(\mathbf{R}_{iw}, \mathbf{k}) \cdot \mathbf{Z}_w \cdot \mathbf{S}_C^{\pm\pm}(\mathbf{R}_{wj}, \mathbf{k}) \cdot \mathbf{T}_{CS}^{\pm-}(\mathbf{k}, l'm'). \quad (110)$$

A physical interpretation of the above relation is straightforward: the spherical components of the flow produced by the particle at point j are transformed into the Cartesian basis by the matrix $\mathbf{T}_{\text{CS}}^{\pm\pm}$; the Cartesian components are propagated by the matrix $\mathbf{S}_{\text{C}}^{\pm\pm}(\mathbf{R}_{\text{wj}})$ to the wall, where they are scattered (as represented by matrix \mathbf{Z}_{w}); the reflected field is propagated to the point i by the matrix $\mathbf{S}_{\text{C}}^{\mp\mp}(\mathbf{R}_{\text{iw}})$; and finally the flow is transformed back into the spherical basis by the matrix $\mathbf{T}_{\text{SC}}^{+\mp}$. We note that, similar to relation (92), the Lorentz symmetry (46) of the matrix elements (110) is explicit due to the symmetry relations (73) and (85) of the component matrices.

Similar to the angular integral in equation (92), the angular integration in the Fourier representation (110) of the matrix \mathbf{G}'_{ij} can be explicitly performed with the help of expressions (68), (88), and (93). The resulting expression for the matrix elements of the one-wall Green operator is

$$G'_{ij}(lm\sigma \mid l'm'\sigma') = \eta^{-1}(-1)^{m'-m} e^{i(m'-m)\phi_{ij}} \times \int_0^\infty g_{\text{w}}^{\pm}(kZ_{\text{iw}}, kZ_{\text{wj}}; lm\sigma \mid l'm'\sigma') k^{l+l'+\sigma+\sigma'-2} J_{m'-m}(k\rho_{ij}) dk, \quad (111)$$

where

$$\mathbf{g}_{\text{w}}^{\pm}(kZ_{\text{iw}}, kZ_{\text{wj}}; lm \mid l'm') = -\tilde{\mathbf{T}}_{\text{SC}}^{+\mp}(lm) \cdot \tilde{\mathbf{S}}_{\text{C}}^{\mp\mp}(kZ_{\text{iw}}) \cdot \mathbf{Z}_{\text{w}} \cdot \tilde{\mathbf{S}}_{\text{C}}^{\pm\pm}(kZ_{\text{wj}}) \cdot \tilde{\mathbf{T}}_{\text{CS}}^{\pm\pm}(l'm'). \quad (112)$$

We recall that the upper signs in the above equations correspond to the fluid occupying the upper half-space Ω^+ , and the lower signs to the fluid in the lower halfspace Ω^- . Taking this into account, we find that the exponential factors resulting from the Cartesian displacement matrices (70) in the product on the right side of equation (112) can be combined into a single exponential factor

$$\mathbf{g}_{\text{w}}^{\pm}(kZ_{\text{iw}}, kZ_{\text{wj}}; lm \mid l'm') \sim e^{-k\Delta_{ij}} \quad (113)$$

where

$$\Delta_{ij} = |Z_{\text{iw}}| + |Z_{\text{wj}}| \quad (114)$$

is the vertical offset between the target point i at the position \mathbf{R}_i and the image of the source point j at

$$\mathbf{R}'_j = \mathbf{R}_j - 2(Z_j - Z_{\text{w}})\hat{\mathbf{e}}_z. \quad (115)$$

It follows that the integrand in equation (111) is the combination of the factor (113), the Bessel function, and powers of k . Thus, relations (96) and (97) imply that the elements of the matrix $\mathbf{g}_{\text{w}}^{\pm}$ can be expressed in terms of the flow produced by an image singularity at $\mathbf{r} = \mathbf{R}'_j$. We note that such a form is required by the Lorentz reflection relation [43]. Explicit expressions for the image force multipole system corresponding to an arbitrary source force mul-

tipole have recently been derived by Cichocki and Jones [20]; we have verified that the integral (111) yields results equivalent to their expressions.

The main application of the Fourier representation of the single-wall Green operator \mathbf{G}'_{ij} is in the subtraction technique that is implemented in our algorithm for evaluating the multiparticle friction matrix in a two-wall system. In this application (in more detail described in Section 8.2) expressions (111) and (112) are used in conjunction with the results of Ref. [20] to accelerate the convergence of the Fourier integrals for the two-wall Green operator.

7 Two-wall Green operator

In this section we generalize the analysis of Section 6 to a system of particles confined between two parallel planar walls. We assume that the walls are in the planes

$$z = Z_L, \quad z = Z_U, \quad (116)$$

where

$$Z_L < Z_U. \quad (117)$$

The suspension occupies the region $Z_L < z < Z_U$. The positions of the walls are indicated by vectors $\mathbf{R}_L = (X_L, Y_L, Z_L)$ and $\mathbf{R}_U = (X_U, Y_U, Z_U)$, where the lateral coordinates X_L and Y_L and X_U and Y_U are chosen arbitrarily.

The flow produced in this system by the induced-force distribution (1) centered at the position of particle j is a superposition of three components

$$\mathbf{v}(\mathbf{r}) = \mathbf{v}_L^{\text{out}}(\mathbf{r}) + \mathbf{v}_U^{\text{out}}(\mathbf{r}) + \mathbf{v}_j^{\text{out}}(\mathbf{r}). \quad (118)$$

Here $\mathbf{v}_j^{\text{out}}(\mathbf{r})$ is the velocity field (11) produced by force distribution \mathbf{F}_j , and $\mathbf{v}_\alpha^{\text{out}}(\mathbf{r})$ is the flow reflected by wall $\alpha = L, U$. By definition, the flow component $\mathbf{v}_L^{\text{out}}(\mathbf{r})$ is nonsingular in the region $z > Z_L$ and vanishes for $z \rightarrow \infty$, and the flow component $\mathbf{v}_U^{\text{out}}(\mathbf{r})$ is nonsingular in the region $z < Z_U$ and vanishes for $z \rightarrow -\infty$. Accordingly, the expansions of the flow fields $\mathbf{v}_L^{\text{out}}$ and $\mathbf{v}_U^{\text{out}}$ in the Cartesian basis sets (50) and (51) have the form

$$\mathbf{v}_L^{\text{out}}(\mathbf{r}) = \int d\mathbf{k} \sum_{\sigma} c_L^{\text{out}}(\mathbf{k}\sigma) \mathbf{v}_{\mathbf{k}\sigma}^{-}(\mathbf{r}_L), \quad (119a)$$

$$\mathbf{v}_U^{\text{out}}(\mathbf{r}) = \int d\mathbf{k} \sum_{\sigma} c_U^{\text{out}}(\mathbf{k}\sigma) \mathbf{v}_{\mathbf{k}\sigma}^{+}(\mathbf{r}_U), \quad (119b)$$

where $\mathbf{r}_L = \mathbf{r} - \mathbf{R}_L$ and $\mathbf{r}_U = \mathbf{r} - \mathbf{R}_U$. Expressions (119) are consistent with the expansion (100b).

The three components (118) of the velocity field produced in the space between the walls by the force distribution \mathbf{F}_j can be used to construct the flow

components $\mathbf{v}_\alpha^{\text{in}}$ ($\alpha = \text{L}, \text{U}$) incoming to wall α . Using expressions (119) and the definition (100a) of the incoming flow we find

$$\mathbf{v}_\text{L}^{\text{in}}(\mathbf{r}) = \mathbf{v}_\text{U}^{\text{out}}(\mathbf{r}) + \mathbf{v}_j^{\text{out}}(\mathbf{r}), \quad (120\text{a})$$

$$\mathbf{v}_\text{U}^{\text{in}}(\mathbf{r}) = \mathbf{v}_\text{L}^{\text{out}}(\mathbf{r}) + \mathbf{v}_j^{\text{out}}(\mathbf{r}). \quad (120\text{b})$$

Relation (11) and the respective decompositions (4) and (118) of the Green function $\mathbf{T}(\mathbf{r}, \mathbf{r}')$ and the flow field $\mathbf{v}(\mathbf{r})$ imply that

$$\mathbf{v}_\text{L}^{\text{out}}(\mathbf{r}) + \mathbf{v}_\text{U}^{\text{out}}(\mathbf{r}) = \int \mathbf{T}'(\mathbf{r}, \mathbf{r}') \cdot \mathbf{F}_i(\mathbf{r}') d\mathbf{r}'. \quad (121)$$

Projecting the above equation onto the reciprocal spherical basis $\mathbf{w}_{lm\sigma}^+$ yields

$$\langle \delta_a^{\text{S}}(i) \mathbf{w}_{lm\sigma}^+(i) | \mathbf{v}_\text{L}^{\text{out}} \rangle + \langle \delta_a^{\text{S}}(i) \mathbf{w}_{lm\sigma}^+(i) | \mathbf{v}_\text{U}^{\text{out}} \rangle = \sum_{l'm'\sigma'} G'_{ij}(lm\sigma | l'm'\sigma') f_j(l'm'\sigma'), \quad (122)$$

which is analogous to the single-wall result (107). Explicit expressions for the matrix elements $G'_{ij}(lm\sigma | l'm'\sigma')$ can thus be derived by generalizing the analysis presented in Section 6.

To this end, the representation of the velocity fields $\mathbf{v}_\alpha^{\text{in}}$ in terms of the Cartesian basis fields $\mathbf{v}_{\mathbf{k}\sigma}^\pm(\mathbf{r}_\alpha)$ aligned with the wall α is obtained by inserting expansions (40) and (119) into (120), and applying the transformation formulas (66) and (76). Using then the single-wall scattering formula (102) to relate the expansion coefficients for the outgoing and incoming flows we get a pair of coupled linear equations

$$\mathbf{c}_\text{L}^{\text{out}}(\mathbf{k}) = -\mathbf{Z}_\text{w} \cdot [\mathbf{S}_\text{C}^{++}(\mathbf{R}_{\text{LU}}, \mathbf{k}) \cdot \mathbf{c}_\text{U}^{\text{out}}(\mathbf{k}) + \eta^{-1} \sum_{l'm'} \mathbf{S}_\text{C}^{++}(\mathbf{R}_{\text{Lj}}, \mathbf{k}) \cdot \mathbf{T}_{\text{CS}}^{+-}(\mathbf{k}, l'm') \cdot \mathbf{f}(l'm')], \quad (123\text{a})$$

$$\mathbf{c}_\text{U}^{\text{out}}(\mathbf{k}) = -\mathbf{Z}_\text{w} \cdot [\mathbf{S}_\text{C}^{--}(\mathbf{R}_{\text{UL}}, \mathbf{k}) \cdot \mathbf{c}_\text{L}^{\text{out}}(\mathbf{k}) + \eta^{-1} \sum_{l'm'} \mathbf{S}_\text{C}^{--}(\mathbf{R}_{\text{Uj}}, \mathbf{k}) \cdot \mathbf{T}_{\text{CS}}^{--}(\mathbf{k}, l'm') \cdot \mathbf{f}(l'm')], \quad (123\text{b})$$

where

$$\mathbf{R}_{\alpha,\beta} = \mathbf{R}_\alpha - \mathbf{R}_\beta \quad \beta = \text{L}, \text{U}, j. \quad (124)$$

In order to express the solution of the system (123) in a compact manner we introduce a matrix notation in the space of six-dimensional vectors of the form

$$\mathbf{c}(\mathbf{k}) = \begin{bmatrix} \mathbf{c}_\text{L}^{\text{out}}(\mathbf{k}) \\ \mathbf{c}_\text{U}^{\text{out}}(\mathbf{k}) \end{bmatrix}. \quad (125)$$

Accordingly, we define the 6×3 and 3×6 transformation matrices

$$T_{CS}(\mathbf{k}, lm) = \begin{bmatrix} \mathbf{T}_{CS}^{+-}(\mathbf{k}, lm) \\ \mathbf{T}_{CS}^{--}(\mathbf{k}, lm) \end{bmatrix}, \quad (126a)$$

$$T_{SC}(lm, \mathbf{k}) = \begin{bmatrix} \mathbf{T}_{SC}^{+-}(lm, \mathbf{k}) & \mathbf{T}_{SC}^{++}(lm, \mathbf{k}) \end{bmatrix}, \quad (126b)$$

the 6×6 Cartesian displacement matrices

$$S_{Wj}(\mathbf{k}) = \begin{bmatrix} \mathbf{S}_C^{++}(\mathbf{R}_{Lj}, \mathbf{k}) & 0 \\ 0 & \mathbf{S}_C^{--}(\mathbf{R}_{Uj}, \mathbf{k}) \end{bmatrix}, \quad (127a)$$

$$S_{iW}(\mathbf{k}) = \begin{bmatrix} \mathbf{S}_C^{--}(\mathbf{R}_{iL}, \mathbf{k}) & 0 \\ 0 & \mathbf{S}_C^{++}(\mathbf{R}_{iU}, \mathbf{k}) \end{bmatrix}, \quad (127b)$$

and the 6×6 two-wall flow reflection matrix

$$Z_{TW}(\mathbf{k}) = \begin{bmatrix} \mathbf{Z}_w^{-1} & \mathbf{S}_C^{++}(\mathbf{R}_{LU}, \mathbf{k}) \\ \mathbf{S}_C^{--}(\mathbf{R}_{UL}, \mathbf{k}) & \mathbf{Z}_w^{-1} \end{bmatrix}^{-1}. \quad (128)$$

For simplicity, the dependence on the wall and particle positions was suppressed on the left side of the above expressions.

Due to the symmetries (73) and (85) of the 3×3 transformation and displacement matrices, the corresponding symmetry relations

$$T_{CS}(\mathbf{k}, lm) = [T_{SC}(lm, \mathbf{k})]^\dagger, \quad (129a)$$

$$S_{Wi}(\mathbf{k}) = [S_{iW}(\mathbf{k})]^\dagger, \quad (129b)$$

$$Z_{TW}(\mathbf{k}) = [Z_{TW}(\mathbf{k})]^\dagger \quad (129c)$$

are satisfied by the matrices (126)–(128). We note that the two-wall scattering matrix (128) involves displacement components describing translation of the flow field between walls.

Using notation introduced above, the solution of the system (123) can be written in the form

$$c(\mathbf{k}) = -\eta^{-1} \sum_{l'm'} Z_{\text{TW}}(\mathbf{k}) \cdot \mathbf{S}_{\text{W}j}(\mathbf{k}) \cdot T_{\text{CS}}(\mathbf{k}, l'm') \cdot \mathbf{f}_j(l'm'). \quad (130)$$

In order to get an explicit expression for the matrix elements of the Green operator \mathbf{G}'_{ij} , equations (119), (122), and (130) are combined, and the scalar products between the Cartesian and spherical basis fields are evaluated with the help of relation (77). The resulting expression for the elements of the two-wall Green matrix is

$$\mathbf{G}'_{ij}(lm | l'm') = -\eta^{-1} \int d\mathbf{k} T_{\text{SC}}(lm, \mathbf{k}) \cdot \mathbf{S}_{i\text{W}}(\mathbf{k}) \cdot Z_{\text{TW}}(\mathbf{k}) \cdot \mathbf{S}_{\text{W}j}(\mathbf{k}) \cdot T_{\text{CS}}(\mathbf{k}, l'm'). \quad (131)$$

The expression is similar in its form (and interpretation) to the corresponding relation (110) for a single-wall system. As with the matrix elements (92) and (110), the Lorentz symmetry (46) of the elements (131) is explicit due to the symmetry relations (129) of the component matrices.

The dependence of the integrand in equation (131) on the polar angles in the Fourier and real spaces is identical to the corresponding dependence in equation (110)—the angular integration can thus be performed in a similar manner. By analogy with equations (111) and (112) we get

$$G'_{ij}(lm\sigma | l'm'\sigma') = \eta^{-1} (-1)^{m'-m} e^{i(m'-m)\phi_{ij}} \times \int_0^\infty g_{\text{TW}}(k; lm\sigma | l'm'\sigma') k^{l+l'+\sigma+\sigma'-2} J_{m'-m}(k\rho_{ij}) dk, \quad (132)$$

where

$$\mathbf{g}_{\text{TW}}(k; lm | l'm') = -\tilde{T}_{\text{SC}}(lm) \cdot \tilde{\mathbf{S}}_{i\text{W}}(k) \cdot \tilde{Z}_{\text{TW}}(k) \cdot \tilde{\mathbf{S}}_{\text{W}j}(k) \cdot \tilde{T}_{\text{CS}}(l'm'), \quad (133)$$

with the matrices in the product given by

$$\tilde{T}_{\text{CS}}(lm) = [\tilde{T}_{\text{SC}}(lm)]^\dagger = \begin{bmatrix} \tilde{\mathbf{T}}_{\text{CS}}^{+-}(lm) \\ \tilde{\mathbf{T}}_{\text{CS}}^{-+}(lm) \end{bmatrix}, \quad (134)$$

$$\tilde{\mathbf{S}}_{\text{W}j}(k) = [\tilde{\mathbf{S}}_{j\text{W}}(k)]^\dagger = \begin{bmatrix} \tilde{\mathbf{S}}_{\text{C}}^{++}(kZ_{\text{L}j}) & 0 \\ 0 & \tilde{\mathbf{S}}_{\text{C}}^{--}(kZ_{\text{U}j}) \end{bmatrix}, \quad (135)$$

and

$$\tilde{\mathbf{Z}}_{\text{TW}}(k) = \begin{bmatrix} \mathbf{Z}_{\text{w}}^{-1} & \tilde{\mathbf{S}}_{\text{C}}^{++}(-kH) \\ \tilde{\mathbf{S}}_{\text{C}}^{--}(kH) & \mathbf{Z}_{\text{w}}^{-1} \end{bmatrix}^{-1}, \quad (136)$$

where

$$H = Z_{\text{U}} - Z_{\text{L}} \quad (137)$$

is the wall separation. The above relations, together with equation (70), imply that $\mathbf{g}_{\text{TW}}(k; lm | l'm')$ depends on the z -coordinates of the walls and the points i and j , but is independent of the lateral coordinates, consistently with the translational invariance of the system. Since the two-wall scattering matrix (136) is more complex than its one-particle counterpart, the integration in equation (132) (unlike (111)) cannot be analytically performed. However, numerical integration is straightforward, except when the lateral distance between points i and j is large, in which case the oscillatory character of the integrand becomes important.

8 Stokesian-dynamics algorithm for suspension between two walls

The theoretical results derived in the previous sections enable development of efficient numerical algorithms for evaluation of many-body hydrodynamic interactions in suspensions of spherical particles confined between two planar walls. To our knowledge, such algorithms have not been available so far. In what follows, we describe a many-particle Stokesian-dynamics algorithm based on our theory.

In Section 8.1 we summarize expressions that relate the matrix \mathbf{M} in the force-multipole equation (48) to the resistance matrix in a suspension of many spheres. Our transformation formulas relating the spherical and Cartesian basis fields are employed in Section 8.2, where a simple numerical-integration procedure for evaluating the elements of the matrix \mathbf{M} is described. The lubrication-subtraction techniques [15, 17, 21] used for improving convergence with the order of the force multipoles included in the calculation are outlined in Section 8.3. Examples of numerical results for the friction matrix of a single particle, a pair of particles, and in many-particle systems are presented in Section 9.

8.1 Resistance matrix

We focus on a system of N spheres undergoing translational and rotational rigid-body motion (7) with no external flow. The particle dynamics in the system is characterized by the resistance matrix

$$\zeta_{ij} = \begin{bmatrix} \zeta_{ij}^{\text{tt}} & \zeta_{ij}^{\text{tr}} \\ \zeta_{ij}^{\text{rt}} & \zeta_{ij}^{\text{rr}} \end{bmatrix}, \quad i, j = 1, \dots, N, \quad (138)$$

defined by the linear relation

$$\begin{bmatrix} \mathcal{F}_i \\ \mathcal{T}_i \end{bmatrix} = \sum_{j=1}^N \begin{bmatrix} \zeta_{ij}^{\text{tt}} & \zeta_{ij}^{\text{tr}} \\ \zeta_{ij}^{\text{rt}} & \zeta_{ij}^{\text{rr}} \end{bmatrix} \cdot \begin{bmatrix} \mathbf{U}_j \\ \boldsymbol{\Omega}_j \end{bmatrix} \quad (139)$$

between the translational and rotational particle velocities \mathbf{U}_j and $\boldsymbol{\Omega}_j$ and the forces and torques \mathcal{F}_i and \mathcal{T}_i applied to the particles. The dot in equation (139) denotes the matrix multiplication and contraction of the Cartesian tensorial components of the resistance matrix. A detailed discussion of a more general resistance problem, which involves an external linear flow and the stresslet induced on the particles, is presented in Ref. [21].

The resistance relation (139) can be linked to the induced-force equation (30) by expressing the applied forces and torques \mathcal{F}_i and \mathcal{T}_i in terms of the induced-force distributions (1),

$$\mathcal{F}_i = \int \mathbf{F}_i(\mathbf{r}) \, d\mathbf{r}, \quad \mathcal{T}_i = \int \mathbf{r}_i \times \mathbf{F}_i(\mathbf{r}) \, d\mathbf{r}. \quad (140)$$

Representing the above quantities in terms of the induced-force multipoles (29) yields

$$\mathcal{F}_i = \sum_{lm\sigma} \mathbf{X}(\mathbf{t} \mid lm\sigma) f(lm\sigma), \quad \mathcal{T}_i = \sum_{lm\sigma} \mathbf{X}(\mathbf{r} \mid lm\sigma) f(lm\sigma), \quad (141)$$

where

$$\mathbf{X}(\mathbf{t} \mid lm\sigma) = \delta_{l1} \delta_{\sigma 0} \tilde{\mathbf{X}}^{\text{t}}(m), \quad (142a)$$

$$\mathbf{X}(\mathbf{r} \mid lm\sigma) = \delta_{l1} \delta_{\sigma 1} \tilde{\mathbf{X}}^{\text{r}}(m). \quad (142b)$$

Explicit expressions for the vectors $\tilde{\mathbf{X}}^{\text{t}}(m)$ and $\tilde{\mathbf{X}}^{\text{r}}(m)$ are listed in Appendix B. The coefficients c_i in the corresponding expansion (36) for the flow field (7) can be represented in the form

$$c_i(lm\sigma) = \mathbf{X}(lm\sigma \mid \mathbf{t}) \cdot \mathbf{U}_i + \mathbf{X}(lm\sigma \mid \mathbf{r}) \cdot \boldsymbol{\Omega}_i, \quad (143)$$

where $\mathbf{v}^{\text{ext}}(\mathbf{r}) = 0$ is assumed. As shown below, the projection matrices \mathbf{X} in equations (141) and (143) obey the identity

$$\mathbf{X}(lm\sigma | A) = \mathbf{X}^*(A | lm\sigma), \quad A = \text{t, r}. \quad (144)$$

In order to determine the resistance matrix ζ_{ij} from the above expressions, the force-multipole equation (48) is solved, which yields the linear relation

$$\mathbf{f}_i(lm) = \sum_{j=1}^N \sum_{l'm'} \mathbf{F}_{ij}(lm | l'm') \cdot \mathbf{c}_j(l'm'), \quad (145)$$

where $\mathbf{F} = \mathbf{M}^{-1}$ is the generalized friction matrix. By inserting into equation (145) the projection formulas (141) and (143) we get

$$\zeta_{ij}^{AB} = \sum_{lm\sigma} \sum_{l'm'\sigma'} \mathbf{X}(A | lm\sigma) F_{ij}(lm\sigma | l'm'\sigma') \mathbf{X}(l'm'\sigma' | B), \quad (146)$$

where $A, B = \text{t, r}$.

With our normalization of the spherical basis fields (16) and (17) (as defined in Section 3.1) the symmetry relation (144) is a direct consequence of the Lorentz symmetry of the generalized friction matrix

$$F_{ij}(lm\sigma | l'm'\sigma') = F_{ji}(l'm'\sigma' | lm\sigma), \quad (147)$$

which follows from equations (45)–(47). Relation (144) is obtained by inserting equation (147) into (146) and using the Lorentz symmetry of the resistance matrix [14]

$$\zeta_{ij}^{AB} = [\zeta_{ji}^{BA}]^\dagger, \quad (148)$$

where the dagger denotes the transposition of a tensor.

8.2 Evaluation of matrix \mathbf{M}

The evaluation of the resistance matrix ζ_{ij}^{AB} from expression (146) requires solving the set of linear algebraic equations for the induced-force multipoles (48) to obtain the generalized friction coefficients $F_{ij}(lm\sigma | l'm'\sigma')$. The matrix \mathbf{M} in the equation (48) is given as the sum of three terms (49). The first two terms, i.e., the single-particle scattering matrix \mathbf{Z}_i and the matrix \mathbf{G}_{ij}^0 representing the flow in infinite space, are known explicitly [41, 37]. The remaining term—the two-wall contribution \mathbf{G}'_{ij} —is evaluated numerically, using relations (132)–(136) along with our expressions for the Cartesian displacement matrices (70), the transformation matrices (90), and the single-wall scattering matrix (103).

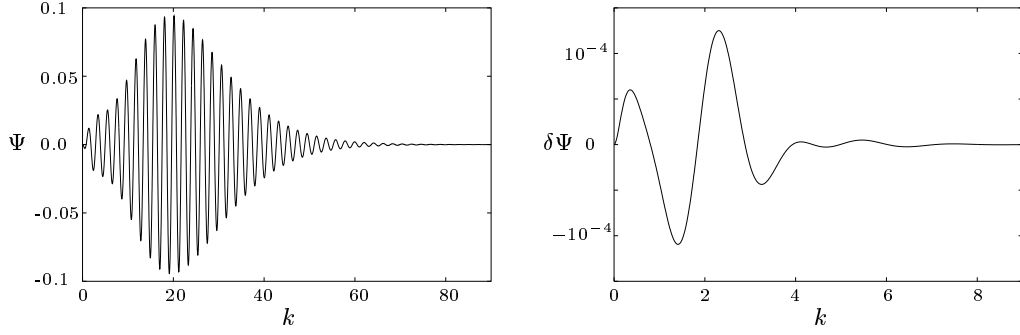


Fig. 1. Integrands Ψ and $\delta\Psi$, defined by equations (149) and (150), versus magnitude of the wave vector k . Separation between walls $H = 1$; distance of the source and target points from lower wall $h_1 = h_2 = 0.1$.

As already mentioned at the end of Section 7, numerical evaluation of the integral (132) is straightforward for sufficiently small lateral separations between particles i and j . For large interparticle separations ρ_{ij} , however, the integration is more difficult because of the oscillatory behavior of the integrands

$$\Psi(k) = g_{\text{TW}}(k; lm\sigma \mid l'm'\sigma') k^{l+l'+\sigma+\sigma'-2} J_{m'-m}(k\rho_{ij}), \quad (149)$$

due to the presence of the factor $J(k\rho_{ij})$. This behavior is illustrated in the left panel of figure 1 for a configuration in which both points i and j are close to one of the walls.

To avoid numerical integration of a highly oscillatory function, the integrand (149) is decomposed

$$\Psi(k) = \Psi_L(k) + \Psi_U(k) + \delta\Psi(k) \quad (150)$$

into the superposition of the single-wall contributions Ψ_L and Ψ_U , and the wall-interaction part $\delta\Psi$. According to equations (111) and (112), the single-wall integrands are

$$\Psi_\alpha(k) = g_w^\pm(kZ_{i\alpha}, kZ_{\alpha j}; lm\sigma \mid l'm'\sigma') k^{l+l'+\sigma+\sigma'-2} J_{m'-m}(k\rho_{ij}), \quad (151)$$

where $\alpha = L, U$. Relation (113) implies that for large values of k the amplitude of these integrands decays as

$$\Psi_\alpha(k) \sim e^{-k\Delta_{ij}^{(\alpha)}}, \quad (152)$$

where $\Delta_{ij}^{(\alpha)}$ is the vertical offset (114) between the point i and the reflection of point j in the wall α . Therefore, the decay is slow if both points i and j are close to the wall, consistent with the results in the left panel of figure 1.

In contrast, the decay of the wall-interaction part $\delta\Psi(k)$ of integrand (150) is determined by the wall separation H . As shown in Appendix D, the large- k

asymptotic behavior of this function is

$$\delta\Psi(k) \sim e^{-k\tilde{\Delta}_{ij}}, \quad (153)$$

where

$$\tilde{\Delta}_{ij} = 2H - |Z_{ij}| > H. \quad (154)$$

The lengthscale $\tilde{\Delta}_{ij}$ equals the vertical offset $|Z_i - Z_j''|$ between the target point i and the closer of the two second-order images of the source point j . The images are at the positions

$$\mathbf{R}_j'' = \mathbf{R}_j \pm 2H\hat{\mathbf{e}}_z, \quad (155)$$

where the plus sign corresponds to reflecting the source point first in the lower wall and then in the upper wall; the minus sign corresponds to the opposite order of reflections.

A typical form of the wall-interaction contribution $\delta\Psi(k)$ is presented in the right panel of figure 1. Unlike the results for $\Psi(k)$, the integrand $\delta\Psi(k)$ in this example is negligible already after several oscillations. Thus, the function $\delta\Psi(k)$ is easy to integrate numerically.

In our algorithm, the contribution $\delta G'_{ij}(lm\sigma | l'm'\sigma')$ to the matrix elements (132), associated with the component $\delta\Psi(k)$ of the integrand, is evaluated by numerical integration using the Simpson rule. The slowly convergent one-wall contributions (151) are calculated analytically, using the explicit image-representation expressions [20] (cf., the discussion in Section 6.2).

Our numerical tests indicate that this procedure yields accurate results for $\rho_{ij}/H \lesssim 20$. The procedure can be further improved, either by subtracting several terms associated with higher-order wall reflections of the source multipole [27], or by deriving asymptotic formulas for the integrals (132).

8.3 Convergence with multipolar order

Our numerical procedure for evaluating the friction matrix involves truncation of the linear system (48) by neglecting the induced force multipoles $\mathbf{f}_i(lm)$ of the order $l > l_{\max}$. This multipolar approximation converges very slowly with the truncation order l_{\max} if any two particles are close together or a particle is close to a wall. Such a behavior stems from a rapid variation of the flow field in the near-contact lubrication regions. The mechanism is well known and has been observed for particles in infinite space and in the presence of a single wall. To overcome this difficulty we employ a standard method, originally introduced by [15], according to which the lubrication forces are included in the friction matrix using a superposition approximation. We follow closely the

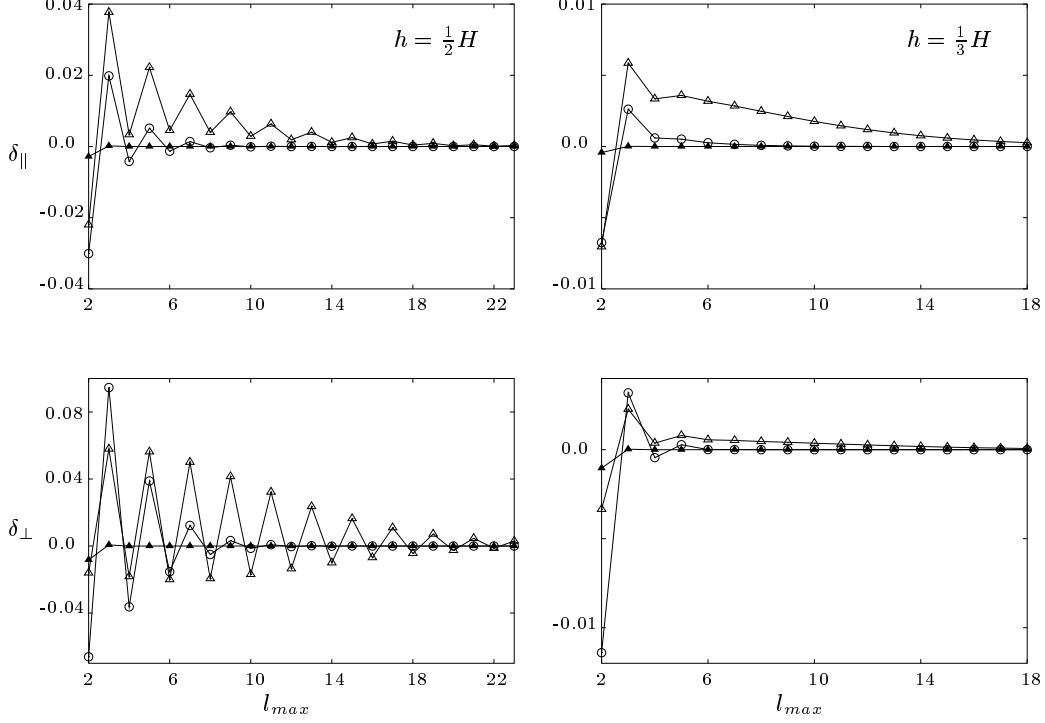


Fig. 2. Relative error δ_α of the lateral ($\delta_{||}$) and vertical (δ_{\perp}) components of the translational friction matrix (160) for a single sphere between two parallel walls, versus truncation order l_{\max} in the multipolar approximation (159). Left panels correspond to center and right panels to off-center particle position (as indicated). Values of dimensionless gap (162) between the particle and the closer wall are $\epsilon_w = 0.02$ (open triangles); $\epsilon_w = 0.1$ (circles); $\epsilon_w = 1.0$ (solid triangles).

implementation of the method described by [21] in their study of a single wall problem. Accordingly, the resistance matrix (138) is represented in the form

$$\zeta_{ij} = \zeta_{ij}^{\text{sup},2} + \zeta_{ij}^{\text{sup},w} + \Delta\zeta_{ij}, \quad (156)$$

where

$$\zeta_{ij}^{\text{sup},2} = \delta_{ij} \sum_{\substack{k=1 \\ k \neq i}}^N \zeta^{(0)}_{ii}(ik) + (1 - \delta_{ij}) \zeta_{ij}^{(0)}(ij) \quad (157)$$

and

$$\zeta_{ij}^{\text{sup},w} = \delta_{ij} [\zeta_i^L(i) + \zeta_i^U(i)]. \quad (158)$$

Here $\zeta_{mm}^{(0)}(mn)$ is the self- and $\zeta_{mn}^{(0)}(mn)$ the mutual-resistance matrix for an isolated pair of particles m and n in the unbounded space, and $\zeta_m^\alpha(m)$ is the single-particle resistance matrix for a sphere in the subspace bounded by the wall $\alpha = L, U$. The superposition contributions (157) and (158) in equation (156) can be calculated with high accuracy, using methods discussed below. The convergence with the truncation order l_{\max} of the multipolar approximation

$$\zeta_{ij} \approx \zeta_{ij}^{\text{sup},2} + \zeta_{ij}^{\text{sup},w} + [\Delta\zeta_{ij}]_{l_{\max}} \quad (159)$$

is much faster than the convergence of the multipolar approximation $[\zeta_{ij}]_{l_{\max}}$ itself, where $[B]_{l_{\max}}$ denotes the quantity B evaluated using the multipolar expansion truncated at $l = l_{\max}$. Therefore the evaluation procedure based on equation (159) yields accurate results for the friction matrix at a substantially reduced numerical cost.

In our implementation, the two-particle components $\zeta_{mm}^{(0)}(mn)$ and $\zeta_{mn}^{(0)}(mn)$ of the friction matrix in the superposition formula (157) are evaluated using a combination of the lubrication resistance expressions [14] and the series expansion in inverse powers of interparticle separation [37]. Similarly, the one-particle friction matrix $\zeta_m^\alpha(m)$ in the superposition formula (158) is evaluated using a combination of the lubrication resistance expression and the power series in the inverse distance of the particle from the wall [20].

Our numerical results indicate that for large and moderate wall separations H (compared to the particle diameter) the multipolar approximation (159) converges rapidly with the truncation order l_{\max} . For configurations with $H \approx 2a$ the convergence is less satisfactory, particularly for the transverse components of the friction matrix. This behavior is illustrated in figure 2, where the relative error for the lateral and vertical components

$$\zeta_{\parallel} = \zeta_{11}^{\text{tt}xx} = \zeta_{11}^{\text{tt}yy}, \quad \zeta_{\perp} = \zeta_{11}^{\text{tt}zz} \quad (160)$$

of the one-particle translational friction matrix is shown for different particle configurations and distances between the walls. The results are given for the center and an off-center position of the particle in the space between the walls,

$$h = \frac{1}{2}H, \quad h = \frac{1}{3}H, \quad (161a, b)$$

where h is the distance of the particle from the lower wall. In the case of the center particle position (161a), the multipole-truncation error exhibits decaying oscillations. For small values of the gap

$$\epsilon_w = h/a - 1 \quad (162)$$

between the particle surface and the closer wall a typical error is in the range of several percent. The results corresponding to truncations at even orders of l_{\max} are more accurate than the results corresponding to truncations at odd orders. The multipolar-truncation error for the off-center particle position (161b) is much smaller than the error for the center configuration with the same values of the particle-wall distance h .

A similar dependence of the truncation error on l_{\max} was observed for many-particle friction matrix: the error is small, except when the wall separation is comparable to the particle diameter. This behavior suggests that the relatively large error for such tight configurations results from an interaction between the lubrication layers—this effect is not accounted for in the superposition terms

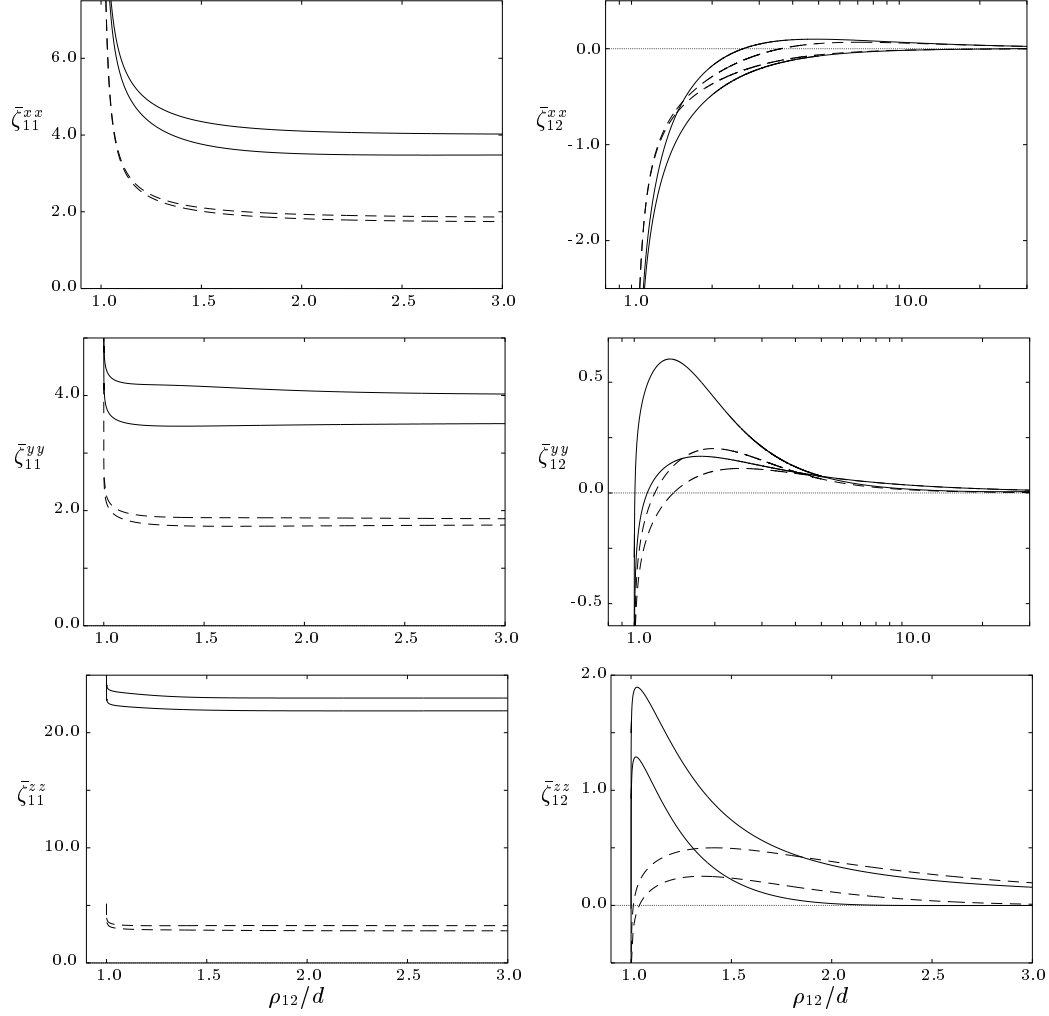


Fig. 3. Normalized translational resistance coefficients (163) for a pair of particles on the x axis in the mid-plane between the walls, versus the interparticle distance ρ_{12} normalized by particle diameter d . Wall separation $H/d = 1.1$ (solid lines); 2.0 (dashed lines). Heavy lines represent the exact results and thin lines the superposition approximation (174).

in equation (159). The problem, however, requires further investigations in order to develop better approximation methods.

9 Numerical results

In this section we give some examples of numerical results for the hydrodynamic friction matrix in systems of spherical particles confined between two parallel planar walls. The calculations for a single particle and for particle pairs, depicted in Figs. 3 and 4, were performed using the multipolar approx-

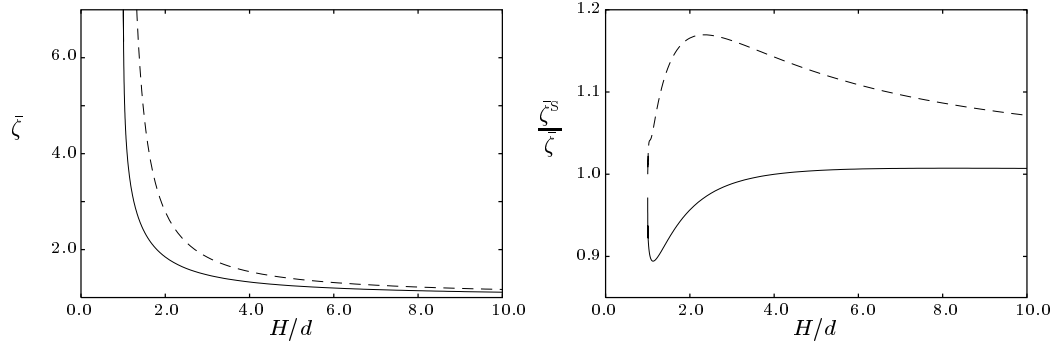


Fig. 4. Normalized one-particle translational resistance coefficients (167) for a particle at the center position in the space between the walls, versus wall separation H normalized by particle diameter d . Horizontal component $\bar{\zeta} = \bar{\zeta}_{\parallel}$ (solid lines); vertical component $\bar{\zeta} = \bar{\zeta}_{\perp}$ (dashed lines). Right panel represents the relative accuracy $\bar{\zeta}^S/\bar{\zeta}$ of the superposition approximation (174).

imation (159) with the truncation at the order $l_{\max} = 12$. The multi-particle calculations, depicted in Figs. 5 and 6, were obtained using $l_{\max} = 8$. These truncations are sufficient to obtain results with the accuracy better than the resolution of the plots. A more extensive set of numerical results is presented in a separate publication [44].

9.1 Two-particle friction matrix

Figure 3 illustrates the behavior of the translational components of the two-particle resistance matrix, normalized by the Stokes friction coefficient $\zeta_0 = 6\pi\eta a$,

$$\bar{\zeta}_{ij}^{\alpha\beta} = \zeta_{ij}^{\text{tt}\alpha\beta} / \zeta_0, \quad i, j = 1, 2, \quad (163)$$

where $\alpha, \beta = x, y, z$. The particle pair is in the center plane of the space between the walls

$$h_1 = h_2 = \frac{1}{2}H, \quad (164)$$

where h_i is the distance of particle i from the lower wall. The relative particle displacement is along the x direction

$$\boldsymbol{\rho}_{12} = \rho_{12} \hat{\mathbf{e}}_x, \quad (165)$$

and the results are plotted versus the interparticle distance ρ_{12} . Only the diagonal Cartesian components $\bar{\zeta}_{11}^{\alpha\alpha}$ and $\bar{\zeta}_{12}^{\alpha\alpha}$ of the self- and mutual-resistance matrices are shown, because $\bar{\zeta}_{ij}^{\alpha\beta} = 0$ for $\alpha \neq \beta$, due to symmetry.

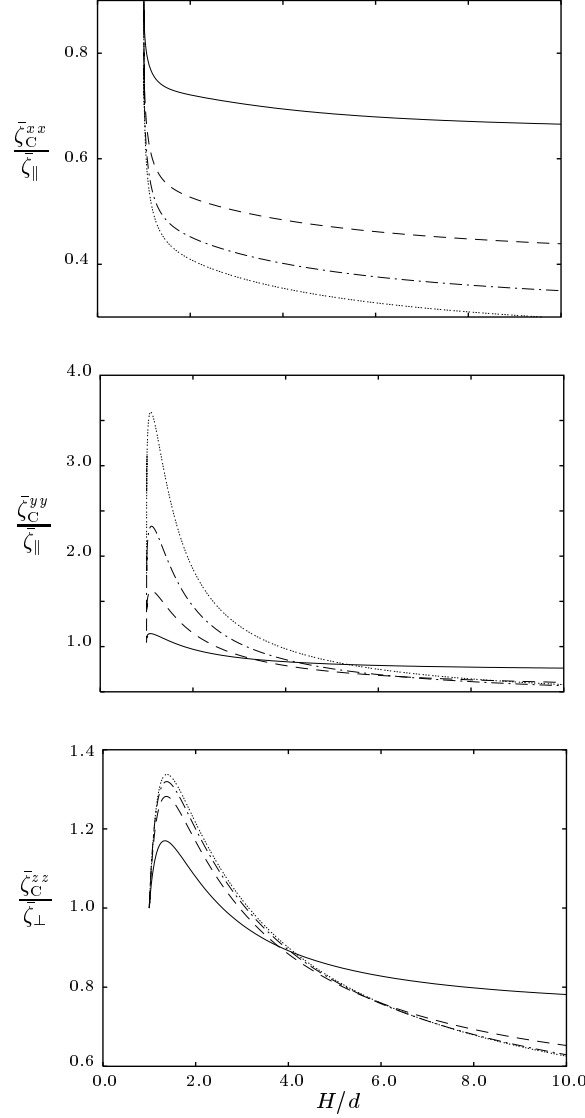


Fig. 5. Translational resistance coefficients per particle (173) of rigid linear arrays of touching spheres on a line parallel to axis x at the center plain between the walls, scaled by corresponding one-particle values (167), versus the wall separation H normalized by particle diameter d . Number of spheres $N = 2$ (solid line); 5 (dashed); 10 (dot-dashed); 20 (dotted).

9.1.1 Near-contact and intermediate behavior

According to the results shown in the left panels of Fig. 3, the self-components of the two-particle resistance matrix are only weakly affected by the presence of the second particle, except for sufficiently small gaps between the particle surfaces

$$\epsilon = \rho_{12}/d - 1, \quad (166)$$

where $d = 2a$ is the particle diameter. The effect of the interparticle interactions is most pronounced for the longitudinal component $\bar{\zeta}_{11}^{xx}$, because of the

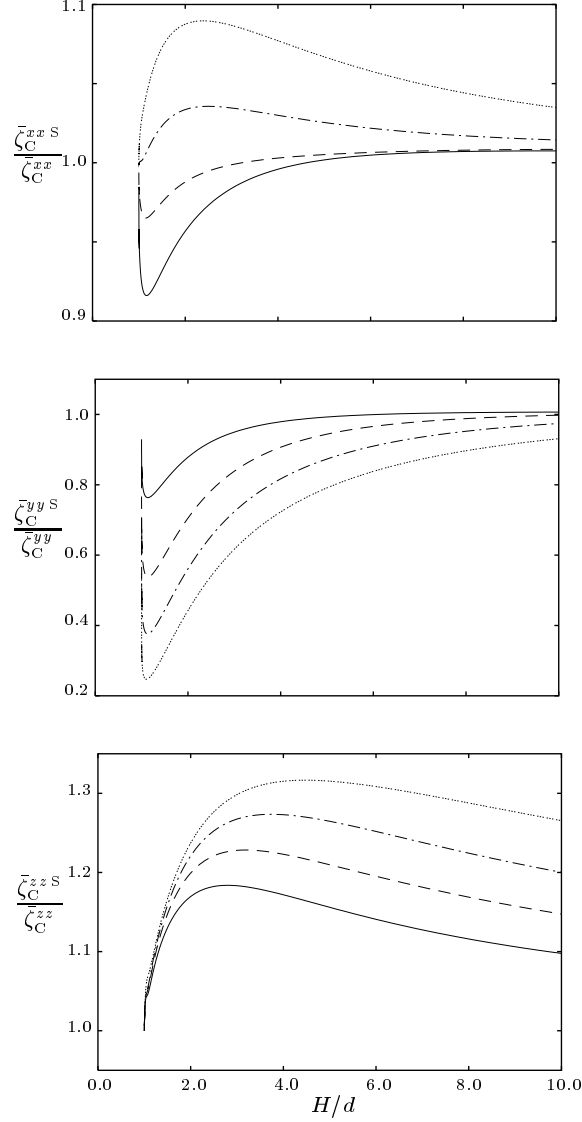


Fig. 6. Same as Fig. (5), but for the relative accuracy $\bar{\zeta}_C^{\alpha\alpha S}/\bar{\zeta}_C^{\alpha\alpha}$ of superposition approximation (174).

strong $O(\epsilon^{-1})$ lubrication resistance for particles in relative motion along the line connecting their centers. For the motion in the transverse directions y and z , a significant interparticle-interaction effect is seen only for very small interparticle gaps, because the transverse interparticle lubrication resistance has a much weaker logarithmic singularity $O(\log \epsilon)$ than the longitudinal one.

The results in the right panels of Fig. 3 indicate that for small interparticle distances all three components $\bar{\zeta}_{12}^{\alpha\alpha}$, $\alpha = x, y, z$, of the mutual friction matrix are negative. The negative sign indicates that the hydrodynamic force $\mathcal{F}_1^H = -\mathcal{F}_1$ produced on particle (1) by the motion of particle (2) points in the same direction as the particle velocity. When the distance between particles is increased, the transverse components $\bar{\zeta}_{12}^{yy}$ and $\bar{\zeta}_{12}^{zz}$ change sign, which results

from the backflow associated with the flow field scattered from the walls. In contrast, the longitudinal component $\bar{\zeta}_{12}^{xx}$ remains negative. We note that the backflow effect does not occur in the unbounded space.

9.1.2 Far-field behavior

At large interparticle separations $\rho_{12}/d \gg 1$, the mutual components $\bar{\zeta}_{12}^{\alpha\alpha}$ of the two-particle resistance matrix vanish, and the self-components $\bar{\zeta}_{11}^{\alpha\alpha}$ tend to the corresponding one-particle values

$$\bar{\zeta}_{\parallel} = \zeta_{\parallel}/\zeta_0, \quad \text{bar}\zeta_{\perp} = \zeta_{\perp}/\zeta_0 \quad (167)$$

($\bar{\zeta}_{\parallel}$ for $\bar{\zeta}_{11}^{xx}$ and $\bar{\zeta}_{11}^{yy}$, and $\text{bar}\zeta_{\perp}$ for $\bar{\zeta}_{11}^{zz}$). The lateral and transverse one-particle friction coefficients $\bar{\zeta}_{\parallel}$ and $\text{bar}\zeta_{\perp}$ are shown in the left panel of Fig. 4 versus the wall separation H for the center particle position $h = \frac{1}{2}H$. Our present one-particle results agree with those of Jones [31] and with our earlier solution obtained using the image-singularity technique [27].

The asymptotic approach of the two-particle friction matrix $\bar{\zeta}_{ij}^{\alpha\alpha}$ to the limiting values at large ρ_{12} can be determined from the far-field behavior of the flow field \mathbf{v}^{as} produced by a particle moving in the horizontal direction \mathbf{e}_{α} ($\alpha = x, y$). By expanding the flow \mathbf{v}^{as} in the small parameter H/ρ , where $\rho \gg H$ is the horizontal distance from the moving particle, we find that

$$\mathbf{v}^{\text{as}} = \frac{1}{2}\eta^{-1}z(H-z)\nabla p^{\text{as}}. \quad (168)$$

Here $z = 0$ is the position of the lower wall, and

$$p^{\text{as}} \sim \frac{\boldsymbol{\rho} \cdot \mathbf{e}_{\alpha}}{\rho^2}, \quad \alpha = x, y, \quad (169)$$

is the pressure field that depends only on the lateral position $\boldsymbol{\rho} = x\hat{\mathbf{e}}_x + y\hat{\mathbf{e}}_y$. The above equation indicates that the far-field velocity (168) decays as

$$\mathbf{v}^{\text{as}} \sim \rho^{-2} \quad (170)$$

for $\rho \rightarrow \infty$. One can also show that the flow field \mathbf{v}^{as} produced by a particle moving in the z direction decays exponentially. The above results are consistent with the asymptotic expression for the flow field produced in the space between the walls by a Stokeslet pointing in the horizontal direction [45]. (A general analysis of the far-field flow will be presented elsewhere.)

The result (170) implies that the asymptotic far-field behavior of the lateral components of the friction matrix is

$$\bar{\zeta}_{11}^{\alpha\alpha} = \bar{\zeta}_{\parallel} + O(\rho_{12}^{-4}), \quad (171)$$

$$\bar{\zeta}_{12}^{\alpha\alpha} = O(\rho_{12}^{-2}), \quad (172)$$

where $\alpha = x, y$ (the $O(\rho_{12}^{-4})$ contribution in Eq. (171) corresponds to the flow field (170) scattered back to the original particle). In contrast to the results (171) and (172), the limits $\bar{\zeta}_{11}^{zz} = \text{bar}\zeta_{\perp}$ and $\bar{\zeta}_{12}^{zz} = 0$ for the vertical components of the friction matrix are approached exponentially on the lengthscale H . The numerical results shown in Fig. 3 agree with the above analysis. In particular, the signs of the longitudinal and transverse friction coefficients $\bar{\zeta}_{12}^{xx}$ and $\bar{\zeta}_{12}^{yy}$ for $\rho_{12}/d \gg 1$ are opposite, consistent with expressions (168) and (169).

9.2 Linear arrays of spheres

In order to illustrate the role of the far-field flow for in wall-bounded systems, we present, in Fig. 5, the resistance function of rigid linear arrays of N touching spheres. The spheres are placed in the mid-plane between the walls on a line pointing in the x direction. The figure shows the diagonal components of the translational resistance matrix of the array treated as a single rigid body

$$\bar{\zeta}_C^{\alpha\alpha} = (N\zeta_0)^{-1} \sum_{i,j=1}^N \zeta_{ij}^{\text{tt}\alpha\alpha}, \quad \alpha = x, y, z. \quad (173)$$

The normalization of the resistance matrix (173) corresponds to the hydrodynamic friction evaluated per one sphere. The results shown in the Fig. 5 are further rescaled by the corresponding one particle results (167), and they are plotted versus the normalized wall separation H/d for several values of the chain length N .

The results in Fig. 5 indicate that for large separations between the walls (compared to the chain length) all three components of the resistance matrix $\bar{\zeta}_C^{\alpha\alpha}$ decrease monotonically with N . Consistent with the behavior of elongated particles in unbounded space [46, 47], we find that $\bar{\zeta}_C^{\alpha\alpha} \sim 1/\log N$ and $\bar{\zeta}_C^{yy} \simeq \bar{\zeta}_C^{zz} \simeq 2\bar{\zeta}_C^{xx}$ for $1 \ll N \ll H/2a$. In contrast, for moderate and small values of the wall separation H the behavior of each component $\bar{\zeta}_C^{\alpha\alpha}$ of the resistance matrix (173) is qualitatively different. The longitudinal component $\bar{\zeta}_C^{xx}$ decreases monotonically with N , while the other two components $\bar{\zeta}_C^{yy}$ and $\bar{\zeta}_C^{zz}$ increase with N due to backflow associated with the presence of the walls. This effect is particularly pronounced for the transverse component $\bar{\zeta}_C^{yy}$, where the increase is by a factor greater than three for $N = 20$ in the regime $H/d \approx 1.2$.

The qualitatively different behavior of the transverse resistance coefficients $\bar{\zeta}_C^{xx}$ and $\bar{\zeta}_C^{yy}$ is associated with the opposite directions of the asymptotic flow field (168) on the horizontal lines parallel and perpendicular to the velocity

of a particle. According to relations (168) and (169), the flow field \mathbf{v}^{as} in front and behind the moving particle points in the direction of the particle velocity. This results in a cooperative effect leading to a reduced resistance per particle for the longitudinal motion of an array. The direction of the flow on the perpendicular line is opposite, which produced a cumulative effect leading to a large increase of the resistance coefficient $\bar{\zeta}_C^{yy}$. This effect is further discussed in Ref. [44].

9.3 Superposition approximation

To illustrate the effect of the hydrodynamic interactions between walls on particle dynamics in wall-bounded systems, the results of our accurate numerical calculations are compared to the single-wall superposition approximation [22, 31, 48]

$$\zeta_{ij}^{\text{S}} = \zeta_{ij}^{\text{L}} + \zeta_{ij}^{\text{U}} - \zeta_{ij}^{(0)}. \quad (174)$$

In the above equation, ζ_{ij}^{L} (ζ_{ij}^{U}) represents the friction matrix for a system of N particles in the presence of the lower (upper) wall, and $\zeta_{ij}^{(0)}$ is the corresponding friction matrix in the absence of the walls. We emphasize that, unlike the superposition terms in equations (156)-(158), all quantities on the right side of equation (174) represent the full N -particle friction matrices—the superposition refers only to the wall contributions. The subtraction of the free-space term $\zeta_{ij}^{(0)}$ assures that the matrix ζ_{ij}^{S} has a correct limit if the distance of the particles to one of the walls (or both walls) tends to infinity.

In Fig. 3, the translational friction coefficients

$$\bar{\zeta}_{ij}^{\alpha\alpha\text{S}} = \zeta_{ij}^{\text{tt}\alpha\alpha\text{S}}/\zeta_0, \quad (175)$$

evaluated in the superposition approximation, are plotted along with the accurate results for the two particle system. The right panel of Fig. 4 represents the ratio $\bar{\zeta}_{11}^{\alpha\alpha}/\bar{\zeta}_{11}^{\alpha\alpha\text{S}}$ for a single particle. The results indicate that the superposition approximation is quite accurate for the single-particle friction coefficients and the self-components of the two-particle friction matrix—the maximal error for these quantities is about 18% (also see the more extensive one-particle calculations reported in Ref. [31]).

The superposition approximation is much less accurate for the mutual components $\bar{\zeta}_{12}^{\alpha\alpha}$ of the two-particle friction matrix, as shown in the right panels of Fig. 3. The accuracy of approximation (174) is especially poor for the transverse component $\bar{\zeta}_{12}^{\alpha\alpha}$ for small values of the wall separation H . Moreover, the approximation yields an incorrect $O(\rho^{-1})$ asymptotic behavior of the mutual friction coefficients for large ρ .

The failure of the superposition approximation is particularly pronounced for the transverse component of the friction coefficient (173) for rigid chains of spheres. As shown in the second panel of Fig. 6, relation (174) grossly underestimates the coefficient $\bar{\zeta}_C^{yy}$ for long chains, especially for small and moderate values of the normalized wall separation H/d . The superposition approximation is insufficient in this regime, because it does not accurately reproduce the far-field interparticle interactions associated with the flow (168).

10 Conclusions

This paper presents results of a theoretical and numerical study of many-body hydrodynamic interactions in suspensions of spherical particles confined between two parallel planar walls. Our primary results include the derivation of transformation relations between spherical and Cartesian basis sets of solutions of Stokes equations. The transformation formulas enable construction of Stokes-flow fields that satisfy appropriate boundary conditions both on the planar walls and on the spherical particle surfaces. Using these transformations, we have developed an efficient numerical procedure for evaluating the many-body resistance matrix characterizing hydrodynamic forces acting on suspension particles in the two-wall geometry.

The basis sets of Stokes flows that are employed in our analysis are closely related to the spherical solutions introduced by Lamb [49] and Cartesian solutions introduced by Faxen [50] (See also section 7.4 of [51]). By a careful choice of the defining properties, however, we have achieved a symmetric matrix formulation of the hydrodynamic-interactions problem. The underlying symmetries of the basis sets include the curl expressions linking the basis fields of different tensorial character, and the diagonal representations of the Oseen tensor in the spherical and Cartesian bases. Exploring the symmetry relations in our canonical formulation, the problem has been reduced to a set of simple explicit expressions.

The results of our theoretical analysis were implemented numerically in an algorithm for evaluating the many-particle resistance matrix in the two-wall system. As a whole, the algorithm is quite complex, because it involves a large number of components. These components include constructing matrix elements of the Green function in terms of lateral Fourier integrals, using subtraction techniques to improve convergence of the integrals for configurations with widely separated particles, solving a linear system of equations for induced-force multipoles, and correcting the solution for slowly convergent lubrication contributions. All the elements in the procedure, however, are either given explicitly or in terms of simple quadratures.

Our numerical algorithm has been used to evaluate the hydrodynamic resistance matrix for a single particle, a pair of particles, and linear arrays of particles confined between two planar walls. The results for the linear arrays indicate that the far-field flow in many-particle systems may produce significant collective effects. A characteristic example is the large hydrodynamic resistance for the transverse motion of an elongated array in a narrow space between the walls. A simple superposition approximation in which the flow scattered from the walls is represented as a combination of two single-wall contributions fails to describe such collective phenomena.

Our current implementation of the Stokesian-dynamics algorithm for suspensions confined between two parallel planar walls allows evaluation of hydrodynamic interactions in a system of about a hundred particles. For a given number of particles, the numerical cost of the method increases with the particle separation (especially for $\rho > 20H$). This increase results from the oscillatory character of the integrands in the Fourier representation of the matrix elements of the Oseen integral operator. The limitation can be removed by subtracting several terms of the multiple-image sequence for the flow produced by the force multipoles induced on the particles. The subtracted contributions can be evaluated explicitly [27].

An alternative and more efficient approach is to use asymptotic expressions for the far-field form of the flow field produced by the force multipoles in the space between the walls. We have recently derived a complete set of such expressions. An important advantage of this approach is its simplicity—the asymptotic multipolar flow fields can be obtained from the solution of the two-dimensional Laplace’s equation for the pressure field in the Hele-Shaw approximation. In particular, algorithms based on this method can be relatively easily generalized for periodic systems. Moreover, the efficiency of such algorithms can be substantially improved by applying the acceleration methods that have been developed for Laplace’s equation [52]. We will describe these results in forthcoming publications.

S. B. would like to acknowledge the support by NSF grant CTS-0201131. E. W. was supported by NASA grant NAG3-2704 and in part by KBN grant No. 5T07C 035 22. J. B. was supported in part by NSF grant cts-s0348175 and in part by Hellman Foundation.

A Spherical basis

In this appendix we list expressions for the reciprocal basis sets (16), (17) and (26), (27) in terms of the normalized vector spherical harmonics, as defined

by Edmonds [40],

$$\mathbf{Y}_{l-1m}(\hat{\mathbf{r}}) = \alpha_l^{-1} r^{-l+1} \nabla \left[r^l Y_{lm}(\hat{\mathbf{r}}) \right], \quad (\text{A.1a})$$

$$\mathbf{Y}_{l+1m}(\hat{\mathbf{r}}) = \beta_l^{-1} r^{l+2} \nabla \left[r^{-(l+1)} Y_{lm}(\hat{\mathbf{r}}) \right], \quad (\text{A.1b})$$

$$\mathbf{Y}_{lm}(\hat{\mathbf{r}}) = \gamma_l^{-1} \mathbf{r} \times \nabla_s Y_{lm}(\hat{\mathbf{r}}). \quad (\text{A.1c})$$

Here

$$Y_{lm}(\hat{\mathbf{r}}) = n_{lm}^{-1} (-1)^m P_l^m(\cos \theta) e^{im\varphi} \quad (\text{A.2})$$

are the normalized scalar spherical harmonics, and the normalization coefficients are

$$\alpha_l = [l(2l+1)]^{1/2}, \quad (\text{A.3a})$$

$$\beta_l = [(l+1)(2l+1)]^{1/2}, \quad (\text{A.3b})$$

$$\gamma_l = -i[l(l+1)]^{1/2}, \quad (\text{A.3c})$$

and

$$n_{lm} = \left[\frac{4\pi}{2l+1} \frac{(l+m)!}{(l-m)!} \right]^{1/2}. \quad (\text{A.4})$$

The vector spherical harmonics (A.1) obey the orthogonality relations

$$\langle \delta(a) \mathbf{Y}_{lnm} | \mathbf{Y}_{l'n'm'} \rangle = \delta_{ll'} \delta_{nn'} \delta_{mm'}. \quad (\text{A.5})$$

The angular functions $\mathbf{V}_{lm\sigma}^\pm$ and $\mathbf{W}_{lm\sigma}^\pm$ in equations (16), (17) and (26), (27) have the following spherical-harmonics expansions

$$\mathbf{V}_{lm\sigma}^\pm = \sum_{\sigma'} \mathbf{Y}_{l-1+\sigma'm} V^\pm(l; \sigma' | \sigma), \quad (\text{A.6a})$$

$$\mathbf{W}_{lm\sigma}^\pm = \sum_{\sigma'} \mathbf{Y}_{l-1+\sigma'm} W^\pm(l; \sigma' | \sigma), \quad (\text{A.6b})$$

The explicit expressions for the matrices \mathbf{V}^\pm at the right side of (A.6) are

$$\mathbf{V}^+(l) = \begin{bmatrix} \alpha_l & 0 & \frac{l}{2(2l+1)} \alpha_l \\ 0 & \frac{i}{l+1} \gamma_l & 0 \\ 0 & 0 & \frac{l}{(l+1)(2l+1)(2l+3)} \beta_l \end{bmatrix} \quad (\text{A.7})$$

and

$$\mathbf{V}^-(l) = \frac{1}{2l+1} \begin{bmatrix} \frac{l+1}{l(2l-1)(2l+1)} \alpha_l & 0 & 0 \\ 0 & i l^{-1} \gamma_l & 0 \\ -\frac{1}{2(2l+1)} \beta_l & 0 & \beta_l \end{bmatrix}. \quad (\text{A.8})$$

Due to orthogonality relations (23) and (A.5), the matrices \mathbf{W}^\pm and \mathbf{V}^\pm satisfy the corresponding orthogonality condition

$$[\mathbf{W}^\pm]^\dagger = [\mathbf{V}^\pm]^{-1}, \quad (\text{A.9})$$

which yields

$$\mathbf{W}^+(l) = \begin{bmatrix} \alpha_l^{-1} & 0 & 0 \\ 0 & -i(l+1)\gamma_l^{-1} & 0 \\ -\frac{(l+1)(2l+3)}{2l}\beta_l^{-1} & 0 & \frac{(l+1)(2l+1)(2l+3)}{l}\beta_l^{-1} \end{bmatrix}, \quad (\text{A.10})$$

$$\mathbf{W}^-(l) = (2l+1) \begin{bmatrix} \frac{l(2l-1)(2l+1)}{l+1}\alpha_l^{-1} & 0 & \frac{l(2l-1)}{2(l+1)}\alpha_l^{-1} \\ 0 & -il\gamma_l^{-1} & 0 \\ 0 & 0 & \beta_l^{-1} \end{bmatrix}. \quad (\text{A.11})$$

In the original publication [37] and in following papers [21, 53], the basis functions $\mathbf{v}_{lm\sigma}^\pm$ and $\mathbf{w}_{lm\sigma}^\pm$ were normalized differently. The relation between the spherical basis fields $\mathbf{v}_{lm\sigma}^{\pm(\text{CFS})}$ and $\mathbf{w}_{lm\sigma}^{\pm(\text{CFS})}$, in the original normalization of Cichocki et al. [37] and the basis introduced in the present paper is

$$\mathbf{v}_{lm\sigma}^-(\mathbf{r}) = N_{l\sigma}^{-1} n_{lm}^{-1} \mathbf{v}_{lm\sigma}^{-(\text{CFS})}(\mathbf{r}), \quad \mathbf{v}_{lm\sigma}^+(\mathbf{r}) = N_{l\sigma} n_{lm}^{-1} \mathbf{v}_{lm\sigma}^{+(\text{CFS})}(\mathbf{r}), \quad (\text{A.12a})$$

$$\mathbf{w}_{lm\sigma}^-(\mathbf{r}) = N_{l\sigma} n_{lm} r \mathbf{w}_{lm\sigma}^{-(\text{CFS})}(\mathbf{r}), \quad \mathbf{w}_{lm\sigma}^+(\mathbf{r}) = N_{l\sigma}^{-1} n_{lm} r \mathbf{w}_{lm\sigma}^{+(\text{CFS})}(\mathbf{r}), \quad (\text{A.12b})$$

where

$$N_{l0} = 1, \quad N_{l1} = -(l+1)^{-1}, \quad l[(l+1)(2l+1)(2l+3)]^{-1}. \quad (\text{A.13})$$

B Transformation vectors \mathbf{X}^t and \mathbf{X}^r

The transformation vectors $\tilde{\mathbf{X}}^t(m)$ and $\tilde{\mathbf{X}}^r(m)$, $m = -1, 0, 1$ in relations (142) are obtained by inserting the multipolar expansion (28) into the definitions (140) and (141). The resulting expressions are evaluated using formulas (27), (A.6b), and (A.10), which yield

$$\tilde{\mathbf{X}}^t(-1) = \left(\frac{2}{3}\pi\right)^{1/2} \begin{bmatrix} 1 \\ -i \\ 0 \end{bmatrix}, \quad \tilde{\mathbf{X}}^t(0) = \left(\frac{2}{3}\pi\right)^{1/2} \begin{bmatrix} 0 \\ 0 \\ \sqrt{2} \end{bmatrix}, \quad \tilde{\mathbf{X}}^t(1) = \left(\frac{2}{3}\pi\right)^{1/2} \begin{bmatrix} -1 \\ -i \\ 0 \end{bmatrix}, \quad (\text{B.1})$$

and

$$\tilde{\mathbf{X}}^r(m) = -2i\tilde{\mathbf{X}}^t(m), \quad m = -1, 0, 1. \quad (\text{B.2})$$

C Elements of transformation matrices $\tilde{\mathbf{T}}_{\text{SC}}^{+\pm}$ and $\tilde{\mathbf{T}}_{\text{CS}}^{\pm-}$

Due to the symmetric formulation of the problem, all four transformation matrices (90) depend on the same set of coefficients (91). Thus, it is sufficient to derive the explicit expression for only one of these matrices. Here we focus on the transformation relation (79) between the Cartesian and spherical basis fields $\mathbf{v}_{\mathbf{k}\sigma}^+$ and $\mathbf{v}_{lm\sigma}^+$.

To find the required transformation formula, we expand $\mathbf{v}_{\mathbf{k}\sigma}^+$ in powers of the radial coordinate r . The expansion can be represented in the form

$$\mathbf{v}_{\mathbf{k}\sigma}^+(\mathbf{r}) = \sum_{n=1}^{\infty} \mathbf{v}_{\mathbf{k}\sigma}^{+(n)}(\mathbf{r}), \quad (\text{C.1})$$

where the fields $\mathbf{v}_{\mathbf{k}\sigma}^{+(n)}(\mathbf{r})$ are homogeneous functions of order n in r . We note that each term in the expansion (C.1) is itself a Stokes flow, because the linear operators in the Stokes equations do not couple terms with different powers of r . It follows that the consecutive expansion terms can be represented as combinations of the spherical basis solutions (17) with $l + \sigma - 1 = n$. For the pressure solution $\mathbf{v}_{\mathbf{k}2}^+$, this representation can be expressed as

$$\mathbf{v}_{\mathbf{k}2}^{+(n)} = \mathbf{u}_{\mathbf{k}2}^{(n)} + \mathbf{u}_{\mathbf{k}1}^{(n)} + \mathbf{u}_{\mathbf{k}0}^{(n)}, \quad (\text{C.2})$$

where

$$\mathbf{u}_{\mathbf{k}\sigma}^{(l+\sigma-1)} = \sum_{m=-l}^l a_{k\sigma}^{lm} \mathbf{v}_{lm\sigma}^+. \quad (\text{C.3})$$

Comparing the above expressions with equations (79), (89), and (90a) yields

$$a_{k\sigma}^{lm} = i^m (2\pi k)^{-1/2} k^{l+\sigma+1} e^{-im\psi} \bar{a}_\sigma, \quad (\text{C.4})$$

where the coefficients a_σ correspond to the coefficients a, b, c in equation (90a),

$$\bar{a}_0 \equiv c, \quad \bar{a}_1 \equiv 2b, \quad \bar{a}_2 \equiv 4a. \quad (\text{C.5})$$

The remaining components $\mathbf{v}_{\mathbf{k}1}^{+(n)}$ and $\mathbf{v}_{\mathbf{k}0}^{+(n)}$ can be related to the flow fields (C.3) by applying the curl operator to both sides of equation (C.1) with $\sigma = 2$ and $\sigma = 1$. After inserting decomposition (C.2) and using curl relations (57) and (20b), we collect terms corresponding to the same power of r , which yields

$$\mathbf{v}_{\mathbf{k}1}^{+(n-1)} = \frac{1}{2} i k^{-1} \nabla \times \left(\mathbf{u}_{\mathbf{k}2}^{(n)} + \mathbf{u}_{\mathbf{k}1}^{(n)} \right), \quad (\text{C.6a})$$

$$\mathbf{v}_{\mathbf{k}0}^{+(n-2)} = -\frac{1}{4}k^{-2}\nabla \times (\nabla \times \mathbf{u}_{\mathbf{k}2}^{(n)}). \quad (\text{C.6b})$$

The above results are consistent with the triangular structure of the transformation matrix (90). To evaluate the coefficients $a_{k\sigma}^{lm}$, we reduce expressions (C.2) and (C.6) to equivalent relations between appropriately defined harmonic scalar fields. For the spherical basis flows $\mathbf{v}_{lm\sigma}^+$ we have

$$\mathbf{v}_{lm\sigma}^+ = \hat{\mathbf{L}}_{l\sigma}^S \Phi_{lm}^+, \quad (\text{C.7})$$

where

$$\Phi_{lm}^+(\mathbf{r}) = r^l Y_{lm}(\hat{\mathbf{r}}), \quad (\text{C.8})$$

and the operators $\hat{\mathbf{L}}_{l\sigma}^S$ are given by

$$\hat{\mathbf{L}}_{l0}^S = \nabla, \quad (\text{C.9a})$$

$$\hat{\mathbf{L}}_{l1}^S = i(l+1)^{-1}\mathbf{r} \times \nabla, \quad (\text{C.9b})$$

$$\hat{\mathbf{L}}_{l2}^S = [(l+1)(2l+3)]^{-1}[-l\mathbf{r} + \frac{1}{2}(l+3)r^2\nabla]. \quad (\text{C.9c})$$

The analogous expressions for the Cartesian basis fields $\mathbf{v}_{\mathbf{k}\sigma}^+$ are

$$\mathbf{v}_{\mathbf{k}\sigma}^+ = \hat{\mathbf{L}}_{k\sigma}^C \Phi_{\mathbf{k}}^+, \quad (\text{C.10})$$

where

$$\Phi_{\mathbf{k}}^+(\mathbf{r}) = (32\pi^2 k)^{-1/2} e^{i\mathbf{k} \cdot \boldsymbol{\rho} + kz}. \quad (\text{C.11})$$

The operators $\hat{\mathbf{L}}_{k0}^C$ and $\hat{\mathbf{L}}_{k1}^C$ are given by the expressions

$$\hat{\mathbf{L}}_{k0}^C = k^{-1}\nabla, \quad (\text{C.12a})$$

$$\hat{\mathbf{L}}_{k1}^C = 2ik^{-1}\hat{\mathbf{e}}_z \times \nabla, \quad (\text{C.12b})$$

and the operator $\hat{\mathbf{L}}_{k2}^C$ is given by

$$\hat{\mathbf{L}}_{k2}^C = \hat{\mathbf{L}}_{k2}^{C1} + \hat{\mathbf{L}}_{k2}^{C2}, \quad (\text{C.12c})$$

where

$$\hat{\mathbf{L}}_{k2}^{C1} = k^{-1}\nabla, \quad \hat{\mathbf{L}}_{k2}^{C2} = -2\hat{\mathbf{e}}_z + 2z\nabla. \quad (\text{C.12d})$$

The above relations can easily be verified using expressions (17) and (A.7) for the spherical basis fields and expressions (51) for the Cartesian basis.

The radial-expansion components $\mathbf{v}_{\mathbf{k}2}^{+(n)}$ in the decomposition (C.1) of the Cartesian basis flows can be determined by applying the operators $\hat{\mathbf{L}}_{k\sigma}^C$ to the expansion of the Cartesian scalar field (C.11) in powers of r

$$\Phi_{\mathbf{k}}^+ = \sum_{n=0}^{\infty} \Phi_{\mathbf{k}}^{+(n)}, \quad (\text{C.13})$$

where

$$\Phi_{\mathbf{k}}^{+(n)}(\mathbf{r}) = (32\pi^2 k)^{-1/2} \frac{(\mathbf{i}\mathbf{k} \cdot \boldsymbol{\rho} + kz)^n}{n!}. \quad (\text{C.14})$$

Inserting relations (C.10) and (C.13) into the expansion (C.1) and collecting terms corresponding to a given power of r we find

$$\mathbf{v}_{\mathbf{k}0}^{+(n)} = \hat{\mathbf{L}}_{k0}^{\text{C}} \Phi_{\mathbf{k}}^{+(n+1)}, \quad \mathbf{v}_{\mathbf{k}1}^{+(n)} = \hat{\mathbf{L}}_{k1}^{\text{C}} \Phi_{\mathbf{k}}^{+(n+1)}, \quad (\text{C.15a, b})$$

and

$$\mathbf{v}_{\mathbf{k}2}^{+(n)} = \hat{\mathbf{L}}_{k2}^{\text{C1}} \Phi_{\mathbf{k}}^{+(n+1)} + \hat{\mathbf{L}}_{k2}^{\text{C2}} \Phi_{\mathbf{k}}^{+(n)}. \quad (\text{C.15c})$$

With the help of relations (C.7)–(C.9) for the spherical basis fields, the flow fields $\mathbf{u}_{\mathbf{k}\sigma}^{(n)}$ in equations (C.6) can be represented in a similar manner,

$$\mathbf{u}_{\mathbf{k}\sigma}^{(l+\sigma-1)} = \hat{\mathbf{L}}_{l\sigma}^{\text{S}} \Psi_{\mathbf{k}\sigma}^{+(l)}, \quad \sigma = 0, 1, 2, \quad (\text{C.16})$$

where

$$\Psi_{\mathbf{k}\sigma}^{+(l)} = \sum_{m=-l}^l a_{k\sigma}^{lm} \Phi_{lm}^+, \quad (\text{C.17})$$

according to equation (C.3).

A closed set of equations for the scalar functions $\Psi_{\mathbf{k}\sigma}^{+(l)}$ is obtained by inserting relation (C.16) into (C.2) and (C.6), using (C.15), and employing the curl identities

$$\mathbf{i}\nabla \times \hat{\mathbf{L}}_{l2}^{\text{S}} \Psi_l = \hat{\mathbf{L}}_{l1}^{\text{S}} \Psi_l, \quad \mathbf{i}\nabla \times \hat{\mathbf{L}}_{l1}^{\text{S}} \Psi_l = \hat{\mathbf{L}}_{l0}^{\text{S}} \Psi_l \quad (\text{C.18a, b}),$$

where Ψ_l is an arbitrary solid harmonic of the order l . The above expressions correspond to the curl identities (19) for the spherical basis fields, and can be verified using relations (C.9). The equations for the scalar functions $\Psi_{\mathbf{k}\sigma}^{+(l)}$ derived by this procedure are

$$\hat{\mathbf{L}}_{l0}^{\text{S}} \Psi_{\mathbf{k}2}^{+(l)} = 4k^2 \hat{\mathbf{L}}_{k0}^{\text{C}} \Phi_{\mathbf{k}}^{+(l)}, \quad (\text{C.19a})$$

$$\hat{\mathbf{L}}_{l0}^{\text{S}} \Psi_{\mathbf{k}1}^{+(l)} = 2k \hat{\mathbf{L}}_{k1}^{\text{C}} \Phi_{\mathbf{k}}^{+(l)} - \hat{\mathbf{L}}_{l-11}^{\text{S}} \Psi_{\mathbf{k}2}^{+(l-1)}, \quad (\text{C.19b})$$

$$\hat{\mathbf{L}}_{l0}^{\text{S}} \Psi_{\mathbf{k}0}^{+(l)} = \hat{\mathbf{L}}_{k2}^{\text{C1}} \Phi_{\mathbf{k}}^{+(l)} + \hat{\mathbf{L}}_{k2}^{\text{C2}} \Phi_{\mathbf{k}}^{+(l-1)} - \hat{\mathbf{L}}_{l-11}^{\text{S}} \Psi_{\mathbf{k}1}^{+(l-1)} - \hat{\mathbf{L}}_{l-22}^{\text{S}} \Psi_{\mathbf{k}2}^{+(l-2)}. \quad (\text{C.19c})$$

The above equations can be explicitly solved for the unknown fields $\Psi_{\mathbf{k}\sigma}^{+(l)}$. Using expressions (C.9) and (C.12) for the operators $\hat{\mathbf{L}}_{l\sigma}^{\text{S}}$ and $\hat{\mathbf{L}}_{k\sigma}^{\text{C}}$, and simplifying the results using relation (C.14) for the field $\Phi_{\mathbf{k}}^{+(l)}$ we find

$$\Psi_{\mathbf{k}2}^{+(l)} = 4k \Phi_{\mathbf{k}}^{+(l)}, \quad (\text{C.20a})$$

$$\psi_{\mathbf{k}1}^{+(l)} = -\frac{4ky}{l}\phi_{\mathbf{k}}^{+(l-1)}, \quad (\text{C.20b})$$

and

$$\psi_{\mathbf{k}0}^{+(l)} = \frac{k[(2l^2 - 4l + 3)(ix + z)^2 + 2(l - 2)z(ix + z) - 2(l - 1)(l - 2)y^2]}{l(l - 1)(2l - 1)}\phi_{\mathbf{k}}^{+(l-2)}, \quad (\text{C.20c})$$

where $\mathbf{k} = k\hat{\mathbf{e}}_x$ is assumed.

In the final step of our derivation, we recall that the functions $\psi_{\mathbf{k}2}^{+(l)}$ are solid harmonics of order l , according to expressions (C.8) and (C.17). To obtain the expansion coefficients $a_{k\sigma}^{lm}$ in relation (C.17) for even values of the parameter $l + m$, we evaluate both sides of (C.20) on the plane $z = 0$ and compare the coefficients of the angular Fourier modes $e^{im\phi}$. In the case of odd values of the parameter $l + m$, a similar analysis is performed for the derivative of both sides of equations (C.20) with respect to the coordinate z . The analysis yields the quantities $a_{k\sigma}^{lm}$ in the form (C.4), with the coefficients (C.5) given by expressions (91).

D Large k behavior of integrands $\delta\Psi(k)$

In this appendix we derive the asymptotic expression (153) for the large k behavior of integrand $\delta\Psi(k)$. According to equations (133) and (149), the decomposition (150) of the integrand $\Psi(k)$ corresponds to the separation

$$\tilde{Z}_{\text{TW}}(k) = \tilde{Z}_0 + \delta\tilde{Z}_{\text{TW}}(k) \quad (\text{D.1})$$

of the two-wall scattering matrix (136) into the $O(1)$ diagonal contribution

$$\tilde{Z}_0 = \begin{bmatrix} \mathbf{Z}_w & 0 \\ 0 & \mathbf{Z}_w \end{bmatrix} \quad (\text{D.2})$$

and the correction of the form

$$\delta\tilde{Z}_{\text{TW}}(k) = -\tilde{Z}_0 \cdot \tilde{S}_{\text{TW}}(k) \cdot \tilde{Z}_{\text{TW}}(k), \quad (\text{D.3})$$

where

$$\tilde{S}_{\text{TW}}(k) = \begin{bmatrix} 0 & \tilde{\mathbf{S}}_{\text{C}}^{++}(-kH) \\ \tilde{\mathbf{S}}_{\text{C}}^{--}(kH) & 0 \end{bmatrix}. \quad (\text{D.4})$$

Taking into account relation (70) we find that

$$\delta\tilde{Z}_{\text{TW}}(k) \sim e^{-kH}, \quad (\text{D.5})$$

which implies that

$$\delta\tilde{Z}_{\text{TW}}(k) \ll \tilde{Z}_0, \quad k \gg 1. \quad (\text{D.6})$$

Inserting the decomposition (D.1) into equations (133) and (149) yields

$$\delta\Psi(k) = \delta g_{\text{TW}}(k; lm\sigma \mid l'm'\sigma') k^{l+l'+\sigma+\sigma'-2} J_{m'-m}(k\rho_{ij}), \quad (\text{D.7})$$

where

$$\delta\mathbf{g}_{\text{TW}}(k; lm \mid l'm') = -\tilde{T}_{\text{SC}}(lm) \cdot \tilde{\mathbf{S}}_{\text{iW}}(k) \cdot \delta\tilde{Z}_{\text{TW}}(k) \cdot \tilde{\mathbf{S}}_{\text{Wj}}(k) \cdot \tilde{T}_{\text{CS}}(l'm'). \quad (\text{D.8})$$

The asymptotic expression (153) is obtained by inserting relation (D.3) with $Z_{\text{TW}}(k) \simeq Z_0$ into (D.8), and using equations (68), (70) and (127). Evaluation of the slowest-decaying term yields (153) with

$$\tilde{\Delta}_{ij} = \min(Z_{iL} + Z_{Uj}, Z_{jL} + Z_{Ui}) + H, \quad (\text{D.9})$$

which is equivalent to (154).

We note that the convergence of the integrand (149) can further be improved by subtracting from the two-wall scattering matrix \tilde{Z}_{TW} several terms in the expansion

$$\tilde{Z}_{\text{TW}}(k) = \sum_{s=0}^{\infty} (-1)^s \tilde{Z}_0 \cdot [\tilde{\mathbf{S}}_{\text{TW}}(k) \cdot \tilde{Z}_0]^s. \quad (\text{D.10})$$

One can show that the subtracted terms correspond to consecutive reflections of the flow field from the walls. Thus, these terms can be evaluated without numerical integration using the image-representation formulas derived by two of us [27].

References

- [1] K. H. Lin, J. C. Crocker, V. Prasad, A. Schofield, D. A. Weitz, T.C. Lubensky, and A.G. Yodh. Entropically driven colloidal crystallization on patterned surfaces. *Phys. Rev. Lett.*, 85:1770, 2000.
- [2] H. Acuña Campa, M. D. Carbajal-Tinoco, J. L. Arauz-Lara, and M. Medina-Noyola. Collective dynamics in quasibidimensional colloidal suspensions. *Phys. Rev. Lett.*, 80:5802–5, 1998.
- [3] R. Pesché, M. Kollmann, and G. Nägele. Brownian dynamics study of dynamic scaling and related freezing criteria in quasi-two-dimensional dispersions. *J. Chem. Phys.*, 114:8701–7, 2001.

- [4] J. Santana-Solano and J. L. Arauz-Lara. Short-time dynamics of colloidal particles confined between two walls. *Phys. Rev. E*, 65:021406–1–8, 2002.
- [5] G. N. Sethumadhavan, A. D. Nikolov, and D. T. Wasan. Stability of liquid films containing monodisperse colloidal particles. *J. Colloid Interface Sci.*, 240:105–12, 2001.
- [6] G. Subramanian, V. N. Manoharan, J. D. Thorne, and D. J. Pine. Ordered macroporous materials by colloidal assembly: A possible route to photonic bandgap materials. *Adv. Mater.*, 11:1261–1265, 1999.
- [7] E. W. Seelig, B. Tang, A. Yamilov, H. Cao, and R. P. H. Chang. Self-assembled 3D photonic crystals from ZnO colloidal spheres. *Mater. Chem. Phys.*, 80:257–63, 2002.
- [8] D. C. Prieve, F. Luo, and F. Lanni. Brownian-motion of a hydrosol particle in a colloidal force-field. *Faraday Discuss. Chem. Soc.*, 83:297, 1987.
- [9] J. Y. Walz and L. Suresh. Study of the sedimentation of a single particle toward a flat plate. *J. Chem. Phys.*, 103:10714–725, 1995.
- [10] L. P. Faucheux and A. J. Libchaber. Confined Brownian motion. *Phys. Rev. E*, 49:5158–63, 1994.
- [11] B. Lin, J. Yu, and S. A. Rice. Direct measurements of constrained Brownian motion of an isolated sphere between two walls. *Phys. Rev. E*, 62:3909–19, 2000.
- [12] T. Palberg and R. Biehl. Sheared colloidal crystals in confined geometry: a real space study on stationary structures under shear. *Faraday Discuss.*, 123:133–43, 2003.
- [13] J. C. Crocker, J. A. Matteo, A. D. Dinsmore, and A. G. Yodh. Entropic attraction and repulsion in binary colloids probed with a line optical tweezer. *Phys. Rev. Lett.*, 82:4352–5, 1999.
- [14] S. Kim and S. J. Karrila. *Microhydrodynamics: Principles and Selected Applications*. Butterworth-Heinemann, London, 1991.
- [15] L. Durlofsky, J. F. Brady, and G. Bossis. Dynamic simulation of hydrodynamically interacting particles. *J. Fluid Mech.*, 180:21–49, 1987.
- [16] A. J. C. Ladd. Hydrodynamic interactions in suspensions of spherical particles. *J. Chem. Phys.*, 88:5051, 1988.
- [17] B. Cichocki, B. U. Felderhof, K. Hinsen, E. Wajnryb, and J. Bławdziewicz. Friction and mobility of many spheres in Stokes flow. *J. Chem. Phys.*, 100:3780–3790, 1994.
- [18] A. S. Sangani and G. B. Mo. An $O(N)$ algorithm for Stokes and Laplace interactions of particles. *Phys. Fluids*, 8:1990–2010, 1996.
- [19] A. Sierou and J. F. Brady. Accelerated Stokesian dynamics simulations. *J. Fluid Mech.*, 448:115–46, 2001.
- [20] B. Cichocki and R. B. Jones. Image representation of a spherical particle near a hard wall. *Physica A*, 258:273–302, 1998.
- [21] B. Cichocki, R. B. Jones, R. Kutteh, and E. Wajnryb. Friction and mobility for colloidal spheres in Stokes flow near a boundary: The multipole method and applications. *J. Chem. Phys.*, 112:2548–61, 2000.

- [22] L. Lobry and N. Ostrowsky. Diffusion of Brownian particles trapped between two walls: Theory and dynamic-light-scattering measurements. *Phys. Rev. B*, 53:12050–6, 1996.
- [23] T. Benesch, S. Yiacoumi, and C. Tsouris. Brownian motion in confinement. *Phys. Rev. E*, 68:021401–1–5, 2003.
- [24] P. Ganatos, S. Weinbaum, and R. Pfeffer. A strong interaction theory for the creeping motion of a sphere between plane parallel boundaries. Part 1. Perpendicular motion. *J. Fluid Mech.*, 99:739–53, 1980.
- [25] P. Ganatos, R. Pfeffer, and S. Weinbaum. A strong interaction theory for the creeping motion of a sphere between plane parallel boundaries. Part 2. Parallel motion. *J. Fluid Mech.*, 99:755–83, 1980.
- [26] M. E. Staben, A. Z. Zinchenko, and R. H. Davis. Motion of a particle between two parallel plane walls in low-Reynolds-number Poiseuille flow. *Phys. Fluids.*, 15:1711–33, 2003.
- [27] S. Bhattacharya and J. Bławdziewicz. Image system for Stokes-flow singularity between two parallel planar walls. *J. Math. Phys.*, 43:5720–31, 2002.
- [28] L. J. Durlofsky and J. F. Brady. Dynamic simulation of bounded suspensions of hydrodynamically interacting particles. *J. Fluid. Mech.*, 200:39–67, 1989.
- [29] P.R. Nott and J.F. Brady. Pressure-driven flow of suspensions—simulation and theory. *J. Fluid Mech.*, 275:157–199, 1994.
- [30] J. F. Morris and J. F. Brady. Pressure-driven flow of a suspension: Buoyancy effects. *Int. J. Multiphase Flow*, 24:105–30, 1998.
- [31] R. B. Jones. Spherical particle in Poiseuille flow between planar walls. *J. Chem. Phys.*, 121:483–500, 2004.
- [32] R. B. Jones. Hydrodynamic interactions of a spherical particle in Poiseuille flow between planar walls. XXI International Congress of Theoretical and Applied Mechanics, August 15–21, 2004, Warsaw, Poland, 2004.
- [33] R. G. Cox and H. Brenner. Effect of finite boundaries on Stokes resistance of an arbitrary particle .3. translation and rotation. *J. Fluid Mech.*, 28:391, 1967.
- [34] P. Mazur and D. Bedeaux. A generalization of Faxén’s theorem to non-steady motion of a sphere through an incompressible fluid in arbitrary flow. *Physica*, 76:235–46, 1974.
- [35] B. U. Felderhof. Force density induced on a sphere in linear hydrodynamics. ii. moving sphere, mixed boundary conditions. *Physica A*, 84:569–576, 1976.
- [36] R. B. Jones and R. Schmitz. Mobility matrix for arbitrary spherical particles in solution. *Physica A*, 149:373–394, 1988.
- [37] B. Cichocki, B. U. Felderhof, and R. Schmitz. Hydrodynamic interactions between two spherical particles. *PhysicoChem. Hyd.*, 10:383–403, 1988.
- [38] J. Bławdziewicz, E. Wajnryb, and M. Loewenberg. Hydrodynamic interactions and collision efficiencies of spherical drops covered with an

- incompressible surfactant film. *J. Fluid Mech.*, 395:29–59, 1999.
- [39] G. S. Perkins and R. B. Jones. Hydrodynamic interaction of a spherical particle with a planar boundary. 1. Free-surface. *Physica A*, 171:575–604, 1991.
 - [40] A. R. Edmonds. *Angular Momentum in Quantum Mechanics*. Princeton University Press, Princeton, 1960.
 - [41] B. U. Felderhof and R. B. Jones. Displacement theorems for spherical solutions of the linear Navier-Stokes equations. *J. Math. Phys.*, 30:339–42, 1989.
 - [42] J. Bławdziewicz, V. Cristini, and M. Loewenberg. Stokes flow in the presence of a planar interface covered with incompressible surfactant. *Phys. Fluids*, 11:251–258, 1999.
 - [43] H. A. Lorentz. A general theory concerning the motion of a viscous fluid. *Abhandl. Theor. Phys.*, 1:23, 1907.
 - [44] S. Bhattacharya, J. Bławdziewicz, and E. Wajnryb. Hydrodynamic interactions of spherical particles in suspensions confined between two planar walls. *J. Fluid Mech.*, in review:xxxx, 2004.
 - [45] N. Liron and S. Mochon. Stokes flow for a stokeslet between two parallel flat plates. *J. Engineering Math.*, 10:287–303, 1976.
 - [46] H. F. Weinberger. Variational properties of steady flow in Stokes flow. *J. Fluid Mech.*, 52:321–44, 1972.
 - [47] J. Bławdziewicz, E. Wajnryb, J. A. Given, and J. B. Hubbard. Sharp scalar and tensor bounds on the hydrodynamic friction and mobility of arbitrarily shaped bodies in Stokes flow. *Phys. Fluids*, xxx:xxx, 2005.
 - [48] R. Pesché and G. Nägele. Stokesian dynamics study of quasi-two-dimensional suspensions confined between two parallel walls. *Phys. Rev. E*, 62:5432–43, 2000.
 - [49] H. Lamb. *Hydrodynamics*. Dover, New York, 1945.
 - [50] H. Faxen. . *Arkiv. Mat. Astron. Fys.*, 17:No. 27, 1923.
 - [51] J. Happel and H. Brenner. *Low Reynolds Number Hydrodynamics*. Martinus Nijhoff, Dordrecht, 1986.
 - [52] D. Frenkel and B. Smit. *Understanding Molecular Simulation. From Algorithms to Simulations*. Academic Press, New York, 2002.
 - [53] J. Bławdziewicz, P. Vlahovska, and M. Loewenberg. Rheology of a dilute emulsion of surfactant-covered spherical drops. *Physica A*, 276:50–80, 2000.